RESEARCH ARTICLE | MARCH 31 2025

Simulation of solar chimney for ventilation of the buildings in Basrah City climate, Iraq FREE

Hussam Hakeem Qasim; Falah A. Abood; Ahmed K. Alshara

AIP Conf. Proc. 3303, 060019 (2025)
https://doi.org/10.1063/5.0262963

Simulation of Solar Chimney for Ventilation of the Buildings in Basrah City Climate, Iraq

Hussam Hakeem Qasim [1, a)], Falah A. Abood [1, b)] and Ahmed K. Alshara [2, c)]

[1] *Department of Mechanical Engineering, College of Engineering, University of Basrah, Basrah, Iraq*.
[2] *Department of Mechanical Engineering, College of Engineering, University of Misan, Misan, Iraq*.

[a)] Corresponding author: pgs.hussam.hakeem@uobasrah.edu.iq
[b)] falah.abood@uobasrah.edu.iq
[c)] dr.ahmed_alshara@uomisan.edu.iq

Abstract. The modern life makes the energy and the source of it is very important, from this renewable energy is solar chimney for natural ventilation, considering the physical properties of the solar radiation and the air in the study area, located in the city of Basrah in southern Iraq, at longitude 47.749° and latitude 30.568°. In the present study the solar chimney with room is simulated numerically using finite volume method with soft package ANSYS – Fluent 2021 / R2. The effect of different inclined angle (α = 30°, 45°, and 60°), the gab of solar chimney (10 cm, 15 cm, and 20 cm) and location of inlet opining (lower, mid, and upper) are investigated. The results are presented as streamline contour, temperature contour and air change per hour ACH. The important results show the optimum ratio of air gap width for solar chimney is 15 cm and tilt angle of solar chimney α = 30° to obtain the maximum ventilation rate and ACH and the location of the air inlet opining at the lower floor for the room gives the best ventilation rate than the other inlet opening locations (mid and upper).

Keywords: Solar Chimney, Ventilation, Air Change per Hour (ACH), Absorber Plate, Inlet Opening Locations.

INTRODUCTION

The solar chimney is one of the modern technologies used to save energy and reduce consumption by utilizing renewable energy (solar energy). Many factors affect the efficiency of the solar chimney, such as the size of the buildings, location of the entrance and exit openings, quality and type of the insulation, as well as the type and shape of the absorber plate, the method of coating it and its type, the dimensions of the solar collector, the height of the ducts, the size of the solar collector, air gab of solar collector, as well as the temperature, the amount of solar radiation and the angle of incidence, as many researches have been conducted on this subject, as the aim of this is to reduce energy consumption, thus lowering the room temperature and reducing the cooling load of air conditioning and this leads to reducing pollution. Not long ago, studies continued for the performance of solar chimney for models conducted on various numerical and experimental applications. Finding the most of the papers use several simulation programs to compare and support experimental results, and this indicates that the method of simulating results is important for predicting and understanding the complex behavior of a solar chimney. Mehani and Settou, (2012) [1] studied numerically the passive cooling using a solar chimney. The change in the width of the chimney and the intensity of solar radiation was studied. The finding illustrated that the solar intensity has a significant effect

The National University of Science and Technology International Conference for Engineering Sciences
AIP Conf. Proc. 3303, 060019-1–060019-28; https://doi.org/10.1063/5.0262963
Published under an exclusive license by AIP Publishing. 978-0-7354-5157-5/$30.00

on the ACH and the flow rate, and the optimum air gap width is (0.2 – 0.3) m to obtain the best ventilation. Hannun et al. (2014) [2] presented numerically the parameters of a solar chimney power plant model, focusing on the impact of collector base shapes, storage material types, and the temperature, velocity, and efficiency. The results suggested that the optimal temperature for the chimney is around 370 K. Shi (2018) [3] analyzed the performance of wall solar chimneys under both cooling and heating modes. findings indicated that the room does not exhibit mixed ventilation with uniform temperature and air density, and the volumetric flow rate influenced by the cavity height and room opening height while the flow rate through sealed heating is dependent on the height of the hot air layer. Abraham and Ming, (2019) [4] studied numerically the design of vertical solar chimney and performance of width for the purpose of increasing the amount of solar radiation. The results showed that the change in the angle and width of chimney led to an increase in the internal wind speed by 10 % when expanding the chimney to 1300 mm. The best performs of chimney when exposed to maximum daylight or a heat flux 800 W/m2. Mohamed et al. (2020) [5] tested the solar chimney influence at different positions and the shape of the partition opening window, namely: on the upper, middle, and lower sides, as well as the horizontal and vertical and square windows. The results showed that the solar chimney with a horizontal suction opening at the bottom of the room at any inclination angle performs is the better ventilation in Maysan – Iraq. Mohammed et al. (2020) [6] investigated the thermal performance of a vertical two-stores solar chimney numerically. Findings revealed that the long vertical solar chimney provided the best natural ventilation but led to noticeable indoor temperature rise. Liu et al. (2021) [7] presented numerically contrastive analysis on the ventilation performance of combined solar chimney. They found that when the ambient temperature ranges from 298 K Up to 303 K in summer, natural ventilation mode is suitable. When the ambient temperature is less than 273K in winter, there is a space heating mode has a better heating effect. Cisse et al. (2022) [8] the optimization of a solar chimney with a horizontal absorber was investigated. Findings indicated that an air velocity of 0.2 m/s can be achieved and the outlet diameter and chimney height significantly influence on the velocity. Yue (2023) [9] investigated numerically the ventilation performance of solar chimneys coupled to outdoor wind and indoor heat sources. The results showed that the maximum ventilation is 32.1% when the solar radiation intensity is 200 W/m^2, outdoor wind speed is 1 m/s, and the indoor heat source increases from 0 to 1500 W/m2. The optimal inlet width for the solar chimney is 0.5 m when considering the effect of outdoor wind. Bassiouny and Koura, (2008) [10] presented a numerically and analytically the solar chimney to improve natural room ventilation. The results showed that the width of the chimney has a greater effect on ACH compared to the size of the chimney inlet. They also found that increasing the inlet size three times leads to improving the ACH by 11%, and increasing the width of the chimney three times leads to increasing the ACH by 25%, keeping the inlet size constant.

Haorong Li et al. (2014) [11] investigated the solar collector with earth – air heat exchangers (EAHEs) for passive air conditioning system. Finding that when the outdoor air temperature and solar radiation increase, the solar chimney natural draft and the amount of airflow to the building increases. Poshtiri and zamiri, (2011) [12] achieved a numerical investigation the ability the solar chimney and earth – air heat exchanger (EAHE). The results showed that the effect of change air gap size on the air change per hour (ACH) with different values of solar radiation has a significant effect up to 0.2 m and the room air temperature remains almost constant after 0.2 m. Abed et al. (2021) [13] studied numerically and experimentally of a solar energy with an EAHE in Tikrit city – Iraq. The finding illustrated that the temperature and air velocity increase with the increase of the solar radiation falling on the wall of the tower, where the maximum drop in air temperature was 18 ℃.

Nakielska and Pawłowski, (2017) [14] investigated experimentally the solar chimney for increasing natural ventilation. The results showed an increase in the exchange and stream of air volume when compared to the situation without the solar chimney. Serageldin et al. (2018) [15] studied experimentally for passive solar chimney heating and ventilation system with EAHE in the cold season in Egypt 14 – 22 March 2019. The finding showed that the optimal chimney design (chimney inclination angle 30° - 35° with the horizontal, length 1.94 - 1.97 m, width 0.92 - 0.97 m, and the gap 0.19 - 0.23 m. They found that the increasing the surface area and aspect ratio of the chimney improves heat transfer and fluid flow, while reducing the gap prevents the appearance of vortices at the leading edge and flow separation at the trailing edge and improves fluid flow. Abdel – Baky et al. (2023) [16] investigated the solar chimneys for natural ventilation, focusing on the cost and environmental impact of conventional energy production. The results finding that the inlet air velocity can remain higher than ambient air velocity during the day and night for several hours, the solar chimneys could achieve natural heating in buildings, and the solar chimneys preserve materials at a stable temperature for long periods after sunset.

Jianliu and Weihua, (2013) [17] presented the room solar chimney in Nanjing, China for a one-story building where simulations were performed using Energy Plus program to predict the performance of the solar chimney. The results showed that an inclination angle of 45° is the most optimal angle for obtaining the maximum ventilation rate, more than a flow rate at inclinations of 30° and 60°, and this ratio increases with increase of the ratio between height of absorber and gap between glass and absorber. Bassiouny and Korah (2009) [18] presented a numerically and analytically the effect of inclination angle of the solar chimney on the ventilation rate and flow pattern, which was simulated using the ANSYS program. The results showed that the optimal value for the flow rate was achieved when the chimney inclination angle is 45° and 70° for latitude 28.4°, and when the increases the inclination angle, the space of inlet flow penetration depth is an increase. In this paper, a proposed solar collector system with the room in Basrah city, Iraq is simulated by ANSYS – Fluent 2021/R2 program. The aim of the current study is in order to find the best ventilation rate by studying several parameters such as the inclination angle of the solar chimney, the air gap between the glass and the heat – absorber plate, and the locations of the entrance holes, the continuity equation, momentum equations, energy equation of air are solved, and obtain the temperature distribution for the system, outlet room temperature, outlet solar collector, solar radiation and ACH.

COMBINATIONAL INVESTIGATION

Geometrical Configuration

Nine models of the room with the solar chimney and conducted with different locations of the inlet openings and the theoretical results were compared with the other research. Fig. 1. shows the solar chimney with room in 2 – dimensional and 3 – dimensional. A three-dimensional model was used to describe the room's problem of natural ventilation. The room was made of wood, cubic size (1×1×1) m, connected at the top by a solar chimney at different angles, and the square inlet room was (0.04) m^2. All room models have the same dimensions of the solar chimney and absorber plate, the difference is in the gab, collector angle, and location of inlet opining. Two layers of wood with a layer of glass wool in the middle are placed behind the absorber plate, the roof and floor of the room to avoid heat transfer from the absorber plate or heat inlet to the room. Table (1) and Table (2) shows materials specifications used in the theoretical analysis of the models and the physical and thermal specifications of the materials, respectively, Table (3) shows the dimensions of the models used, where their properties were examined in the laboratories of the College of Engineering – Department of Mechanics - University of Basrah and the Southern Technical University - Basrah Engineering Technical College.

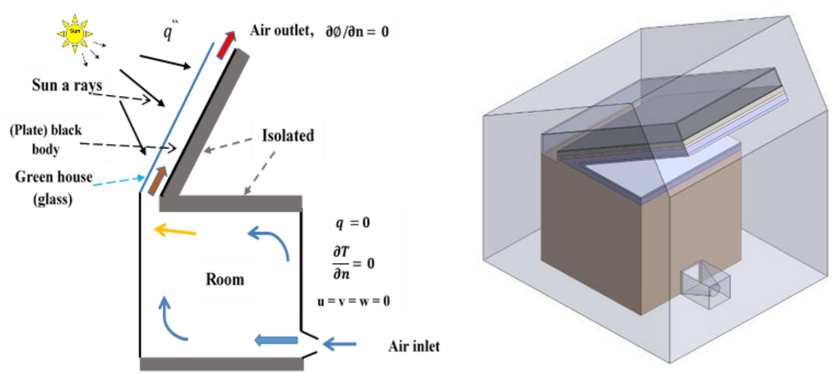

FIGURE 1. Schematic diagram for the model 2D (left) and 3D (right)

TABLE 1. Materials specifications

Description	Item	Symbol	Value
Aluminum sheet	Length	L_{AS}	1.5 m
	Width	w_{AS}	1 m
	Thickness	t_{AS}	1mm
Glass	Thickness	t_g	4 mm
Wood	Thickness	w_d	18 mm
Glass wool	Thickness	t_{gw}	5 cm

TABLE 2. Physical and thermal properties

Materials	Density (ρ) (kg/m^3)	Thermal Conductivity (k) (W/m.K)	Specific heat capacity (C_P) (J/kg.K)
Glass Wool	12	0.04	840
Aluminum Sheet	2645	220.68	864.35
Glass	2220	1.15	830
Wood	721	0.159	1260
Air	1.225	0.0242	1005

TABLE 3. The basic parameters for the prototype models

Basic Parameter of the Prototype	Value
Solar collector gap	0.1 m, 0.15 m, 0.2 m
Solar collector length	1.5 m
Solar collector width	1 m
Dimension of solar collector outlet	0.15 m × 1 m
Glass thickness	4 mm
Area of solar collector roof	1.5 m^2
Aluminium plate length	1.5 m
Aluminium plate width	1 m
Aluminium plate thickness	1 mm
Solar chimney angle	30°, 45°, 60°
Glass wool insulation thickness	5 cm
Glass wool insulation thickness in the base of the room	5 cm
Glass wool insulation thickness in the roof of the room	5 cm
Volume of the cooling room	1 m^3
Cooling room inlet diameter	10.16 cm
Dimension of the inlet opening at the wall of the room	0.2 m × 0.2 m
Dimension of the room outlet opening	0.15 m × 1 m
Wood thickness	18 mm

The Governing Equations

The air flow in the solar chimney is caused by natural convection that results from solar radiation. The governing equations used in the simulation consist of mass conservation for the Reynolds Averaged Navier–Stokes (RANS) equations, the energy, turbulence and radiation transfer equations. The governing equations (continuity, momentum, and energy) in the system were solved by using several assumptions to solve the present flow and heat transfer cases. These assumptions for the solar chimney with the room as the following:

A. Unsteady state conditions for solar chimney with the room.
B. Turbulent flow.
C. Three-dimensional model.
D. Density in buoyancy force is modeled by Boussinesq approximation is utilized.
E. Insulated walls of room is exposed to the solar radiation, and the room is subjected to different thermal boundary conditions along the test day:

$$\left(\frac{\partial T}{\partial x} \neq 0, \frac{\partial T}{\partial y} \neq 0\right)$$

- The flow is incompressible.

F. No-slip conditions between the fluid and wall.
G. All the air properties are constant and they are evaluated at ambient temperature T_a = 300 K.

H. Viscous dissipation and compression work are assumed negligibly small.
I. The solar chimney with the room facing south at 30.568738° latitude and longitude 47.749277°.

The governing equations are a set of Kronecker symbol δ_{ij}, for continuity, momentum, and energy equations as shown below [19]:

- Continuity equation

$$\frac{\partial \rho}{\partial t} + \frac{\partial u_i}{\partial x_i} = 0 \tag{1}$$

The other fundamental set of equations that govern fluid flow is derived from Newton's second law (conservation of momentum). The equations are called Navier-Stokes equations, and for the flow of incompressible fluids.

- Momentum equation

$$\rho \frac{Du_i}{Dt} = -\frac{\partial P}{\partial x_i} + \frac{\partial}{\partial x_j}\left[\mu\left(\frac{\partial u_i}{\partial x_j} + \frac{\partial u_j}{\partial x_i}\right) - \rho\overline{u_i^` u_j^`}\right] + \rho g_i \beta (T - T_a) \tag{2}$$

- Energy equation

Represents the transport of heat within the flow field.

$$\rho C_P \frac{DT}{Dt} = \frac{\partial}{\partial x_j}\left[k\frac{\partial T}{\partial x_j} - \rho C_P \overline{u_j^` T^`}\right] \tag{3}$$

$$\frac{DT}{Dt} = \frac{\partial}{\partial x_j}\left[\frac{k}{\rho C_P}\frac{\partial T}{\partial x_j} - \overline{u_j^` T^`}\right] \tag{4}$$

$$\frac{DT}{Dt} = \frac{\partial}{\partial x_j}\left[\alpha\frac{\partial T}{\partial x_j} - \overline{u_j^` T^`}\right] \tag{5}$$

$$\alpha = \frac{k}{\rho C_P} \tag{6}$$

Where:

$$\frac{D}{Dt} = \frac{\partial}{\partial t} + u\frac{\partial}{\partial x} + v\frac{\partial}{\partial y} + w\frac{\partial}{\partial z} \tag{7}$$

$$\frac{DT}{Dt} = \frac{\partial T}{\partial t} + u\frac{\partial T}{\partial x} + v\frac{\partial T}{\partial y} + w\frac{\partial T}{\partial z} \tag{8}$$

x_j = x, y, z and u_j = u, v, w

Know the finial energy equation becomes:

$$\frac{\partial T}{\partial t} + u\frac{\partial T}{\partial x} + v\frac{\partial T}{\partial y} + w\frac{\partial T}{\partial z} = \frac{\partial}{\partial x}\left(\alpha\frac{\partial T}{\partial x}\right) + \frac{\partial}{\partial y}\left(\alpha\frac{\partial T}{\partial y}\right) + \frac{\partial}{\partial z}\left(\alpha\frac{\partial T}{\partial z}\right) \tag{9}$$

The Eq. (7) called the material derivative [20]. $\rho g \beta (T - T_a)$: is the buoyancy source or sink term. with τ the viscous stress tensor: u_i is the velocity components in the directions X_i, X_j. T, P temperature and pressure respectively. μ is viscosity, $\rho\overline{u_i^` u_j^`}$ is turbulent Reynold's stress. $\rho\overline{u_j^` T^`}$ the turbulent heat transfer is evaluated by an opposite turbulence model. By adopting the eddy or turbulent viscosity models are calculated as [21]:

turbulent Reynolds stresses:

$$-\rho\overline{u_i^` u_j^`} = \mu_t\left(\frac{\partial u_i}{\partial x_j} + \frac{\partial u_j}{\partial x_i}\right) - \frac{2}{3}\rho k \delta_{ij} \tag{10}$$

turbulent heat transfer:

$$-\rho\overline{u_j^` T^`} = \frac{\mu_t}{Pr_i}\frac{\partial T}{\partial x_j} \tag{11}$$

Where: μ_t is the turbulent dynamic viscosity**,** *Pr* the Prandtl number. δij Kronecker delta, δij = 1 if i=j and δij = 0 if i $\neq$j.

TURBULENCE MODEL

To express turbulent heat fluxes and turbulent viscosity stresses (Reynolds stresses), many turbulence models have used the concept of turbulent viscosity or turbulent diffusion [22]. The Turbulence Model (RNG k-epsilon Model) is based on the renormalization group analysis of the Navier–Stokes equations proposed by Orszag 1993 [23]. This model contains an additional expression in the turbulent energy dissipation rate equation, and the effect of eddy flow has also been taken into account in this model. Therefore, it gives good accuracy for eddy flows. The transport equations for kinetic turbulence and dissipation are the same as those for the standard k-ε model, but the model constants are different and the constant $C_{\varepsilon 1}$ is replaced by the function $C_{\varepsilon 1 RNG}$. The transport equation for turbulence dissipation becomes as follows [24,25]:

1. Turbulence kinetic energy (k):

$$\frac{\partial}{\partial t}\ (\rho k) + \frac{\partial}{\partial x_i}\ (\rho k u_i) = \frac{\partial}{\partial x_i}\left(\frac{\mu}{\sigma_{kRNG}}\frac{\partial k}{\partial x_i}\right) + \mu_t\left(\frac{\partial u_i}{\partial x_j} + \frac{\partial u_j}{\partial u_i}\right)\frac{\partial u_i}{\partial x_j} - \rho\varepsilon \tag{12}$$

2. Dissipation rate (ε)

$$\frac{\partial}{\partial t}(\rho\varepsilon) + \frac{\partial}{\partial x_i}(\rho\varepsilon u_i) = \frac{\partial}{\partial x_j}\left[\left(\mu + \frac{\mu_t}{\sigma_{\varepsilon RNG}}\right)\frac{\partial \varepsilon}{\partial x_j}\right]\frac{\varepsilon}{k}\ (C_{\varepsilon 1RNG}\ G + C_{\varepsilon 2RNG}\ \rho\varepsilon) \tag{13}$$

$$\mu_t = \frac{C_\mu \rho k^2}{\varepsilon} \tag{14}$$

$$C_{\varepsilon 1RNG} = 1.42 - f_\eta \tag{15}$$

$$f\eta = \frac{\eta\left(1 - \frac{\eta}{4.38}\right)}{(1 + \beta_{RNG}\eta^3)} \tag{16}$$

$$\eta = \sqrt{\frac{G}{\rho C_{\mu RNG}\varepsilon}} \tag{17}$$

$$G = \mu_t\left[2\left(\left(\frac{\partial u}{\partial x}\right)^2 + \left(\frac{\partial v}{\partial y}\right)^2 + \left(\frac{\partial w}{\partial z}\right)^2\right) + \left(\frac{\partial u}{\partial y} + \frac{\partial v}{\partial x}\right)^2 + \left(\frac{\partial u}{\partial z} + \frac{\partial w}{\partial x}\right)^2 + \left(\frac{\partial v}{\partial z} + \frac{\partial w}{\partial y}\right)^2\right] \tag{18}$$

$$G = \mu_t\ \left(\frac{\partial u_i}{\partial x_j} + \frac{\partial u_j}{\partial u_i}\right)\frac{\partial u_i}{\partial x_j} \tag{19}$$

Where: k is the turbulence kinetic energy, and is defined as the variance of the fluctuations in velocity, μ is viscosity, μ_t is the eddy or turbulent viscosity, $f\eta$, η turbulent model coefficient, G: is the generation of turbulent kinetic energy due to the mean velocity gradient or shear [26]. The constants of the turbulence model are given in Table (4).

TABLE 4. Constants for the RNG (k – ε) model

$C_{\varepsilon 2RNG}$	β_{RNG}	$C_{\mu RNG}$	$\sigma_{\varepsilon RNG}$	σ_{kRNG}	C_μ
1.68	0.012	0.0845	0.7179	0.7179	0.09

INITIAL AND BOUNDARY CONDITIONS

In any appropriate attempt to solve any problem there must be application of boundary conditions. The initial condition for the temperature of the solar chimney with the room was (300 K) at inlet room and (309 K) for the ambient temperature. A schematic diagram of the solar boundary conditions for the geometrical symmetric shape as it is shown in the Fig. (2), and based on the preceding assumptions, the boundary and initial condition for the turbulent flow for the system:

Initial Conditions:

- For the temperature: all exterior walls with ambient conditions $T = T_a$ = 309 K and temperature for inlet room T_{in} = 300 K for all cases.
- For the velocity: as pressure inlet P_{in} = zero-gauge pressure.
- The kinetic energy and dissipation rate at inlet distribution, the rough approximation for the turbulence kinetic energy k and dissipation rate ε in internal flow can be obtained from the turbulence intensity Ti and the characteristic length of duct L by means of the following simple assumed [20]:

$$k = \frac{2}{3}(u_{in}Ti)^2 \tag{20}$$

$$\varepsilon = C_\mu^{\frac{3}{4}}\ \frac{k^{\frac{3}{2}}}{l} \tag{21}$$

$$l = 0.07\,L \tag{22}$$

Where: Ti is turbulence intensity and equal = 0.05, l is the depth of chimney or room height, and u_{in} is the reference mean flow velocity. [27].

Boundary Conditions:

- The outlet boundary condition: pressure outlet boundary at atmospheric pressure (P_{out} = 0).
- Boundaries surfaces of the top of the room and backside of chimney are insulated:

$\frac{\partial T}{\partial n} = 0$ where: n = x, y, and z direction.

- No slip walls u, v, w = 0.
- All contact surfaces between the surface of the room and solar chimney with air, and all interior walls with continuous boundary conditions are:

$$T_{sarface} = T_{air} \longrightarrow \left(-k\frac{\partial T}{\partial n}\right)_{surface} = \left(-k\frac{\partial T}{\partial n}\right)_{air}$$

- The solar chimney with room were subjected to solar ray (I) and it change with time and the intensity of solar radiation.
- The kinetic energy of turbulent and the rate of dissipation at the exit:

$$\left.\frac{\partial k}{\partial x}\right|_{y=L} = \left.\frac{\partial \varepsilon}{\partial x}\right|_{y=L} = 0 \quad (23)$$

- The outer domain that around the room and solar chimney is the ambient air with $T = Ta$.

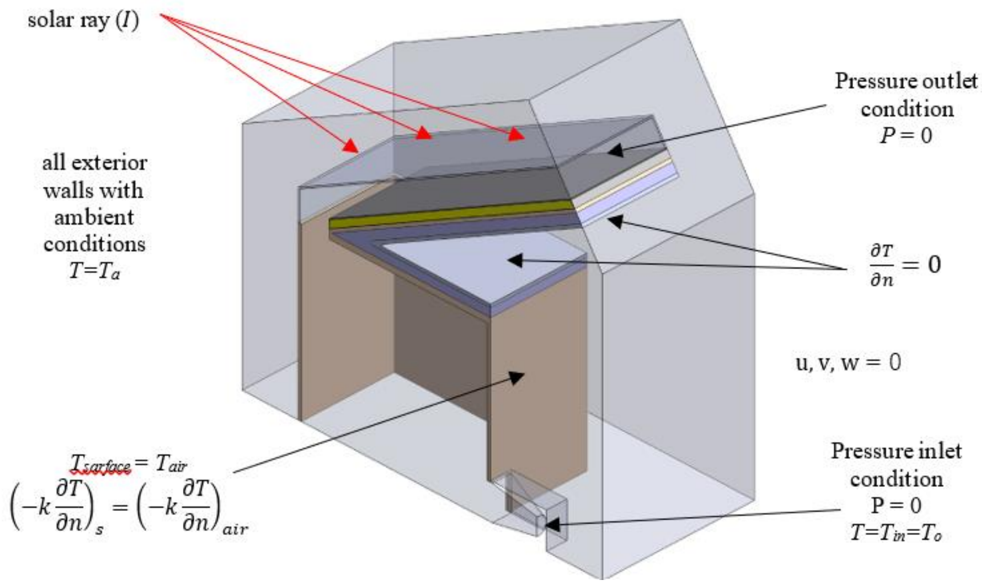

FIGURE 2. Boundary types of domains in symmetric shape

THE MESH

Mesh Generation

The initial stage of the finite volume approach involves the creation of the grid. Mesh modeling is a prominent concern that has several applications in the field of computational fluid dynamics. The process of meshing directly affects the accuracy and convergence of the computational fluid dynamics (CFD) simulation results [28]. The generated model was fragmented into smaller components using basic form elements that were linked at shared nodes using the ANSYS Fluent simulation program. The tetrahedron were chosen for this study because of the complex geometry. Higher mesh quality yields more accurate findings, but lower mesh quality, up to a specific threshold, leads to insufficient results. The Fig. 3 depicts the solar chimney with room displays different sorts of 3D mesh elements used in ANSYS-Fluent 2021/ R2.

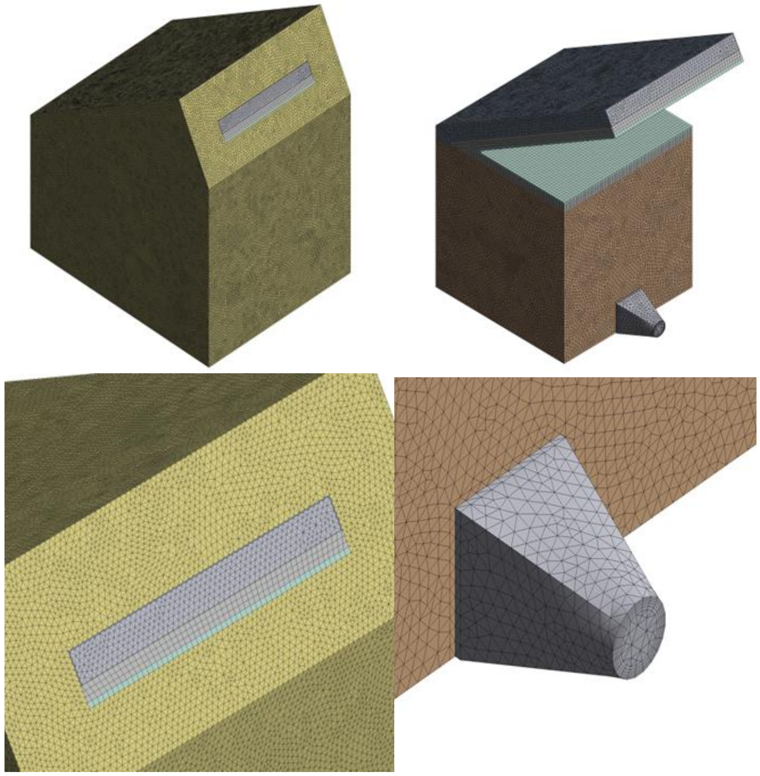

FIGURE 3. The mesh generation for the model with display the inlet and outlet openings

Mesh Independence Test

In order to ascertain that the results are solely influenced by the boundary conditions and physics employed, rather than the mesh resolution, it is imperative to do a mesh independence analysis in Computational Fluid Dynamics (CFD). A commonly used approach to assess grid independence involves systematically increasing the resolution and conducting repeated simulations. If the results do not significantly alter, it is likely that the initial grid is sufficient. Calculations have been performed for five specific grid sizes. The findings of the grid independence test for the room with solar chimney are summarized in Table (5).

It was noted that the number of elements 2385058 and 3112521 were nearly identical. Therefore, a domain consisting of 2385058 elements was selected in order to enhance computational accuracy and minimize calculation time. Fig. 4 displays the variation of number of elements with ACH.

The Fluent code employs powerful numerical analytic techniques and various approaches to obtain optimal results. The current study utilizes the CFD software ANSYS – Fluent 2021/R2 to solve the given model. The process of solving using Fluent involves the following flow chart as shown is figure (5).

TABLE 5. Grid independence test

Mesh	No. of element	ACH
Mesh – 1	925441	40.802
Mesh – 2	1126521	41.108
Mesh – 3	1504108	42.665
Mesh – 4	2385058	43.847
Mesh – 5	3112521	44.01

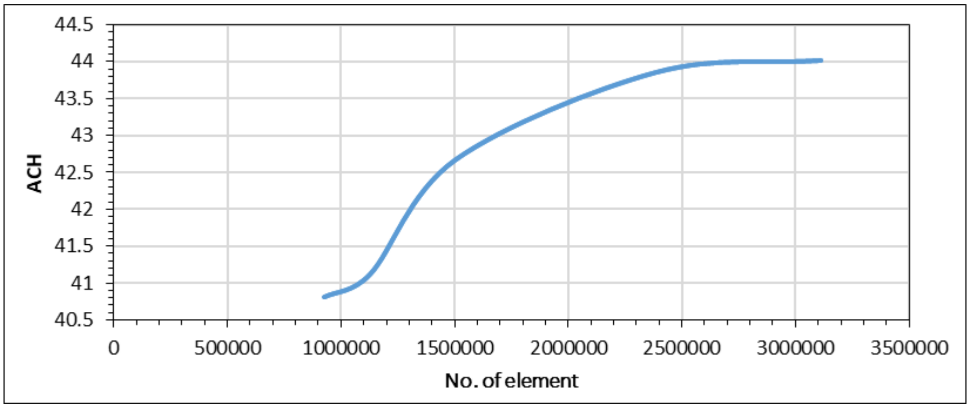

FIGURE 4. Variation of Air Change per Hour (ACH) with total elements number

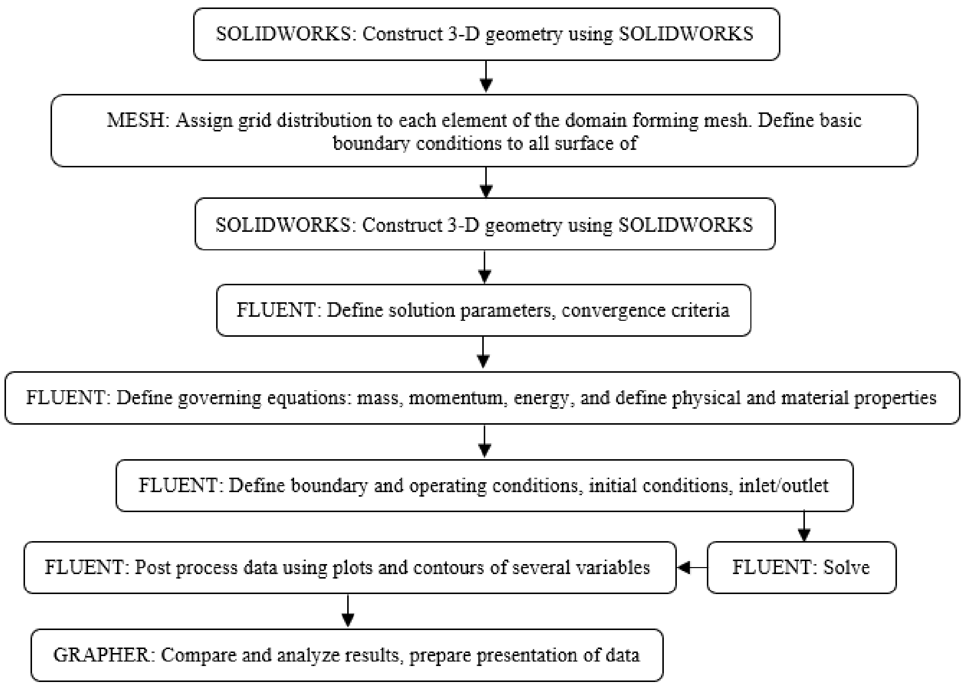

FIGURE 5. Flow-chart for numerical solution by ANSYS – Fluent 2021/ R2 software

NUMERICAL RESULTS VALIDATION

For the purpose of validating the solution of simulating the numerical model of the solar chimney with the room in the ANSYS – Fluent 2021/R2 program, the results of several studies by Mathur et al. [29], B and K [30], and Park [31] were used. The current data was compared with previous numerical and experimental data [29,30,31] as shown in Fig. 6 and Table (6). The results show a good agreement between the numerical results and other researcher. For the purpose of ACH calculation, there is an acceptable error between the expected data and the measurements, as the error rate for the ACH account was 3.16 %, which is a value that falls within the range of errors and is considered a relatively low value.

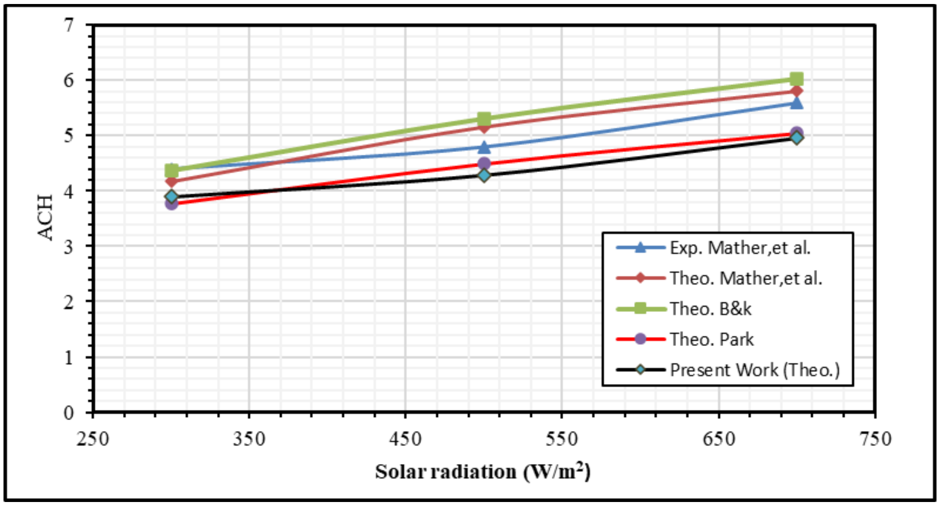

FIGURE 6. Variation of solar radiation with ACH, solar radiation angel $\beta = 55°$, comparing with simulations and experiments for previous studies

TABLE 6. Summary of ACH for present work comparing with simulations and experiments for previous studies

Air gap (m)	**Chimney inlet (height) (m)**	**I (W/m^2)**	**ACH**					**Error% With Park [30]**
			Exp. Mathur et al. [29]	**Theo. Mathur et al. [29]**	**Theo. B&K [10]**	**Theo. Park [30]**	**Theo. Present work**	
0.3	0.3	300	4.4	4.17	4.37	3.77	3.89418	3.2938
		500	4.8	5.16	5.31	4.49	4.286604	4.5299
		700	5.6	5.81	6.03	5.04	4.95648	1.6571

RESULTS AND DISCUSSION

In this piper, the room unit integrated with a solar collector was presented, and its performance was numerically analysis. The numerical analysis in this study was performed depend on Basrah city climate (longitude 47.749° and latitude 30.568° and it is placed facing south) in Iraq by using ANSYS – Fluent 2021/R2 software. The results of solar chimney with the room, performance of solar chimney, including the angle difference, the air gap, inlet location and other relevant factors are presented. All the models of cases subjected to the average inlet temperature to the solar chimney is 300 K, ambient temperature is 309 K, atmospheric pressure and exposed to solar radiation. The models are studied in order to find the enhance of the ventilation rate in each one. The following cases are shown in details and disused:

- Case (1): Air gap for solar chimney = 10 cm, where three angles of the solar chimney are taken: 30°, 45°, and 60°.
- Case (2): Air gap for solar chimney = 15 cm, where three angles of the solar chimney are taken: 30°, 45°, and 60°.
- Case (3): Air gap for solar chimney = 20 cm, where three angles of the solar chimney are taken: 30°, 45°, and 60°.
- Case (4): Different inlet opening location for the room, which are the lower, mid and upper inlet.

Figure (7) shows the contours of streamline for the solar chimney with room, the numerical study was performed at gab = 10 cm, different time 9 a.m., 12 p.m., 3 p.m. and 6 p.m. with different tilt angle for solar collector ($\alpha = 30°$, 45°, 60°) and for varying solar intensity were exposed along the daylight. For $\alpha = 30°$, at 9 a. m., it can be noted that the streamlines become freer in the chimney because the wide gab which gives small effect on the magnitude of temperature and velocity, this returns to cross section of inlet opening. For $\alpha = 30°$, at 12 p. m., it can be noted that the streamlines become dense and larger than that at 9 a.m. in the chimney because the gab was small. For $\alpha = 30°$, at 3 p. m., it can be seen that the streamlines become freer and with big vorticity in the chimney because less ventilation rate. For α = 30°, at 6 p. m., it can be seen that the streamlines become freer and with less dense and formed a large vorticity in the chimney because less ventilation rate. For α = 45°, it can be seen from the figure that the best flow lines are at 12 p.m., where they are straight, and they are also inside the room and more density, this is due to the fact that at 12 p.m., the intensity of solar radiation is the maximum possible, and the intensity of solar radiation begins to decrease after 12 p.m., there will be difficulty in escaping the air from the solar collector, and vortices will form that impede the movement of the air. For α = 60°, It can be seen from this figure that the best flow lines are at 12 p.m., where they are less straight from α = 30° and 45°. However, inside the room, the streamlines will be large, density and close together at 3 p.m. Figure (8) shows the contours of streamline for the solar chimney with room, the numerical study was performed at gab = 15 cm, different time 9 a.m., 12 p.m., 3 p.m. and 6 p.m. with different tilt angle for solar collector (α = 30°, 45°, 60°) and for varying solar intensity were exposed along the daylight. For α = 30°, at 9 a. m., it can be noted that the streamlines become freer in the chimney because the wide gab which gives small effect on the magnitude of temperature and velocity, this returns to cross section of inlet opening. For α = 30°, at 12 p. m., it can be noted that the streamlines become freer and larger than that at 9 a.m. in the chimney because the wide gab which gives small effect on the magnitude of temperature and velocity. For α = 30°, at 3 p. m., it can be seen that the streamlines become freer and with vorticity in the chimney because less ventilation rate and the wide gab which gives small effect on the magnitude of temperature and velocity. For α = 30°, at 6 p. m., it can be seen that the streamlines become freer and with large vorticity in the chimney because less ventilation rate and the wide gab which gives small effect on the magnitude of temperature and velocity. For α = 45°, it can be seen from the figure that the best flow lines are at 12 p.m., where they are straight, and they are also less inside the room, this is due to the fact that at 12 p.m., the intensity of solar radiation is the maximum possible, and the intensity of solar radiation begins to decrease after 12 p.m., there will be difficulty in escaping the air from the solar collector, and vortices will form that impede the movement of the air. However, inside the room, the streamlines will be large, density and close together at 6 p.m. For α = 60°, It can be seen from this figure that the best flow lines are at 6 p.m., due to the increased height of the solar chimney, where they are less straight from α = 30° and 45°, and they are also less inside the room for the air flow, some vortices are formed at the outlet of the solar chimney due to the increased angle to 60° at 12 p.m., and at that time the intensity of solar radiation is the maximum possible, and the intensity of solar radiation begins to decrease after 12 p.m., there will be difficulty in escaping the air from the solar collector, and vortices will form more than that at α = 30° and 45° that cause the impede the movement of the air. However, inside the room, the streamlines will be large, density and close together at 3 p.m. Figure (9) shows the contours of streamline for the solar chimney with room, the numerical study was performed at gab = 15 cm, different time 9 a.m., 12 p.m., 3 p.m. and 6 p.m. with different tilt angle for solar collector (α = 30°, 45°, 60°) and for varying solar intensity were exposed along the daylight. For α = 30°, it can be noted that the streamlines become freer in the chimney because the wider gab which gives small effect on the magnitude of temperature and velocity, and the best flow lines are at 12 p.m., after that time the vortices are formed in the outlet of solar chimney. there will be difficulty in escaping the air from the solar collector, and vortices will form that impede the movement of the air. However, inside the room, the streamlines will be large, density and close together at 6 p.m. especially on the floor of the room and the beginning of the inlet opening of solar collector, due to the inability of air to exit the room due to the formation of vortexes. For α = 45°, it can be noted that the streamlines become freer in the chimney because the wider gab which gives small effect on the magnitude of temperature and velocity, the streamlines at 9 a.m., 12 p.m. are almost identical, but there is density in the flow lines at 9 a.m. due to the large vortexes formed in the solar collector, which try to prevent the mass flow rate to exit from solar collector. With increasing time at 6 p.m., the streamlines become dense, especially on the floor of the room, the side opposite the inlet air into the room. there will be difficulty in escaping the air from the solar collector, and vortices will form that impede the movement of the air. However, inside the room, the streamlines will be large and density. For α = 60°, it can be seen from this figure that the best flow lines are at 9 a.m., due to the increased height of the solar chimney and increased the gab of solar collector where they are more straight from α = 30° and 45° for the same gab, and less vortex formation inside the room, some vortices are formed at the outlet of the solar chimney due to the increased angle to 60° at 6 p.m., and decreases solar radiation, at that time the intensity of streamlines are increase there will be difficulty in escaping the air from the solar collector, and vortices will form less than that at α = 30° and 45° contrary when the gap was 10 cm and 15 cm. However, inside the room, the streamlines will be large, density and close together at 3 p.m. Figure (10) shows the contours of temperature for the solar chimney with room, the numerical study was performed at gab = 10 cm, different time 9 a.m., 12 p.m., 3 p.m. and 6 p.m. with different tilt angle for solar collector (α = 30°, 45°, 60°) and for varying solar intensity were exposed along the daylight. When the angle is 30°, we notice a decrease in temperature after 12 p.m., due to decrease in solar radiation. For α =

45°, the maximum temperature is 357.188 K, and the temperature begins to decrease in the same behavior as before. As for the surface temperature, it increases with decrease in the rate of solar radiation due to a decrease in the ventilation rate. For α = 60°, it is clear from this figure that the maximum temperature was 353.677 at 12 p.m. and it begins to decrease until it becomes 335.239 K. It can be seen from the figure that the maximum temperature of the absorbent plate is at an angle of 45°, and the minimum temperature is at the same angle as well. Figure (11) shows the contours of temperature for the solar chimney with room, the numerical study was performed at gab = 15 cm, different time 9 a.m., 12 p.m., 3 p.m. and 6 p.m. with different tilt angle for solar collector (α = 30°, 45°, 60°) and for varying solar intensity were exposed along the daylight. α = 30°, at 9 a.m., it can be noted that the temperature of plate collector was maximum 346.154 K, which present the driven bouncy force to flow inside the room. α = 30°, at 12 p.m., the temperature of plate collector was maximum 360.919 K, which present the driven bouncy force to flow inside the room was increases. α = 30°, at 3 p.m., the temperature of plate collector was maximum 349.753 K. α = 30°, at 6 p.m., the temperature of plate collector was maximum 334.902 K, this decreases for the temperature because of decrease of solar radiation. For α = 45°, it can be seen from this figure the maximum temperature was 360.773 K at noon 12 p.m., because the solar radiation is maximum at the midday and the temperature begins to decrease due to decrease the solar radiation, until it becomes (333.732 K) in the evening at 6 p.m., which present the driven bouncy force to flow inside the room. Also, the high temperature at the surface of heat absorbing plate for collector and extended to the celling of room. This temperature increases on the surface as solar radiation decreases over time, and this temperature is due to the decrease in the ventilation rate resulting from the decrease in solar radiation. The thermal plume near the absorber tend to move out the chimney for high intensity while less for low intensity due to the high absorber temperature led to encourages buoyancy force. The warm air is enclosing at the upper zone since warm air arises and no venting at the upper zone. The temperature of the wood is high at high flux solar intensity that effect on the heat transfer to the room. In addition, that the solar radiation has a major effect since the solar radiation transmit through the glass to the heat absorber plate. For α = 60°, It can be seen from this figure the maximum temperature was 356.772 K at noon 12 p.m., because the solar radiation is maximum at the midday and the temperature begins to decrease due to decrease the solar radiation, until it becomes 333.932 K in the evening at 6 p.m., which present the driven bouncy force to flow inside the room. Also, the high temperature at the surface of heat absorbing plate for collector and extended to the celling of room. As for the temperature of the solar collector outlet, it becomes lower than the temperature when the angles are 30° and 45° due to the increase in the angle. This temperature increases on the surface as solar radiation decreases over time, and this temperature is due to the decrease in the ventilation rate resulting from the decrease in solar radiation. The warm air is enclosing at the upper zone since warm air arises and no venting at the upper zone It is most intense in the evening at 6 p.m. The temperature of the wood is high at high flux solar intensity that effect on the heat transfer to the room. Figure (12) shows the contours of temperature for the solar chimney with room, the numerical study was performed at gab = 20 cm, different time 9 a.m., 12 p.m., 3 p.m. and 6 p.m. with different tilt angle for solar collector (α = 30°, 45°, 60°) and for varying solar intensity were exposed along the daylight. For α = 30°, it can be seen from this figure the maximum temperature was 358.356 K at noon 12 p.m., because the solar radiation is maximum at the midday and the temperature begins to decrease due to decrease the solar radiation, until it becomes 334.649 K in the evening at 6 p.m., which present the driven bouncy force to flow inside the room. Also, the high temperature at the surface of heat absorbing plate for collector and extended to the celling of room. This temperature increases on the surface as solar radiation decreases over time, and this temperature is due to the decrease in the ventilation rate resulting from the decrease in solar radiation. The warm air is enclosing at the upper zone since warm air arises and no venting at the upper zone. The temperature of the wood is high at high flux solar intensity that effect on the heat transfer to the room. For α = 45°, it can be realized from this figure the maximum temperature was (357.091 K) at noon 12 p.m., because the solar radiation is maximum at the midday and the temperature begins to decrease due to decrease the solar radiation, until it becomes (333.306 K) in the evening at 6 p.m., which present the driven bouncy force to flow inside the room. Also, the high temperature at the surface of heat absorbing plate for collector and extended to the celling of room. This temperature increases on the surface as solar radiation decreases over time, it is concentrated on the upper surface of the room, at 6 p.m. and this temperature is due to the decrease in the ventilation rate resulting from the decrease in solar radiation. Also, the lowest temperature is at the air entry hole into the room and the floor. For α = 60°, it can be seen from this figure the maximum temperature was 357.398 K at noon 12 p.m., because the solar radiation is maximum at the midday and the temperature begins to decrease due to decrease the solar radiation, until it becomes 333.982 K in the evening at 6 p.m., which present the driven bouncy force to flow inside the room. Also, the high temperature at the surface of heat absorbing plate for collector and extended to the celling of room. As for the temperature of the solar collector outlet and temperature of absorber plate, it becomes lower than the temperature when the angles are 30° and 45° due to the increase in angle. This temperature increases on the surface as solar radiation decreases over time, and this temperature is due to the decrease in the ventilation rate resulting from the decrease in solar radiation. Figure (13) shows the contours of streamline, velocity, and temperature for the solar chimney with the room when gab = 15 cm, α = 30° and 12 p.m. and different inlet location (lower, mid and upper). It can be noted that the streamlines at lower inlet become freer and straight with the formation of small eddies compared to the locations of the middle and upper inlet openings, the streamlines at the location of the lower inlet are clear and heading directly to the exit opening from the room to the solar collector. As for the location of the upper opening, large eddies are formed because the air entering is colder than the air inside the room, and so are eddies in the solar collector. It can be notice from the figure that the air flow velocity increases with closer the inlet opening to the floor, meaning that the lower inlet is the best ventilation rate, knowing that all opening locations have a relatively close ventilation rate, but the best is the location of the lower inlet opening. The obstruction to the ventilation rate or the air velocity exchange results from the direction of the air inside the room due to the change in the locations of the openings, where the cold air descends to the bottom of the room and then when it warms it heads to the room outlet, this is indicated by the distribution of temperatures, as we notice that the average temperature in the lower inlet opening is the lowest possible, and then it begins to increase gradually as the location of the inlet opening increases. This shows that the ventilation rate in the lower opening is the highest possible due to the decrease in temperatures in the room.

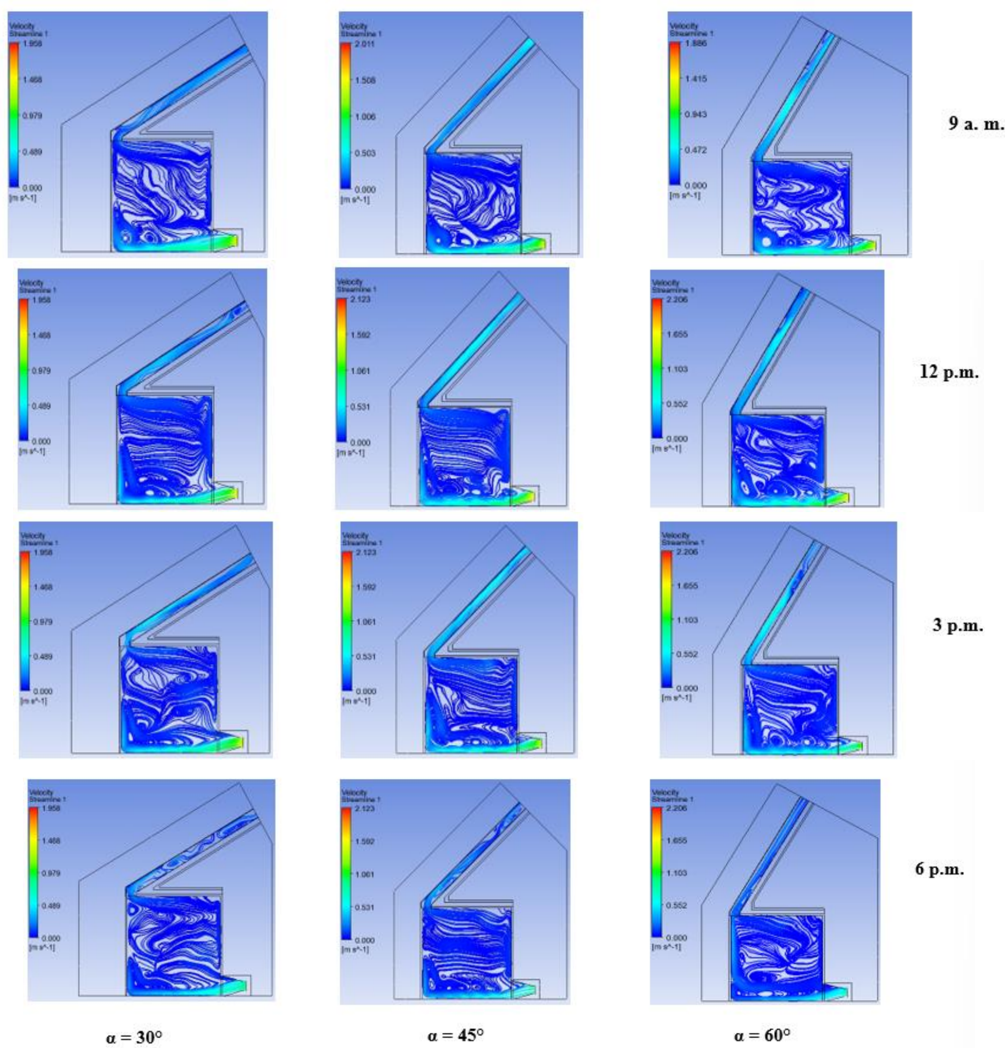

FIGURE 7. Contours illustrate the streamlines for the room and solar chimney at gab = 10 cm, different tilt angle of solar collector and with different time

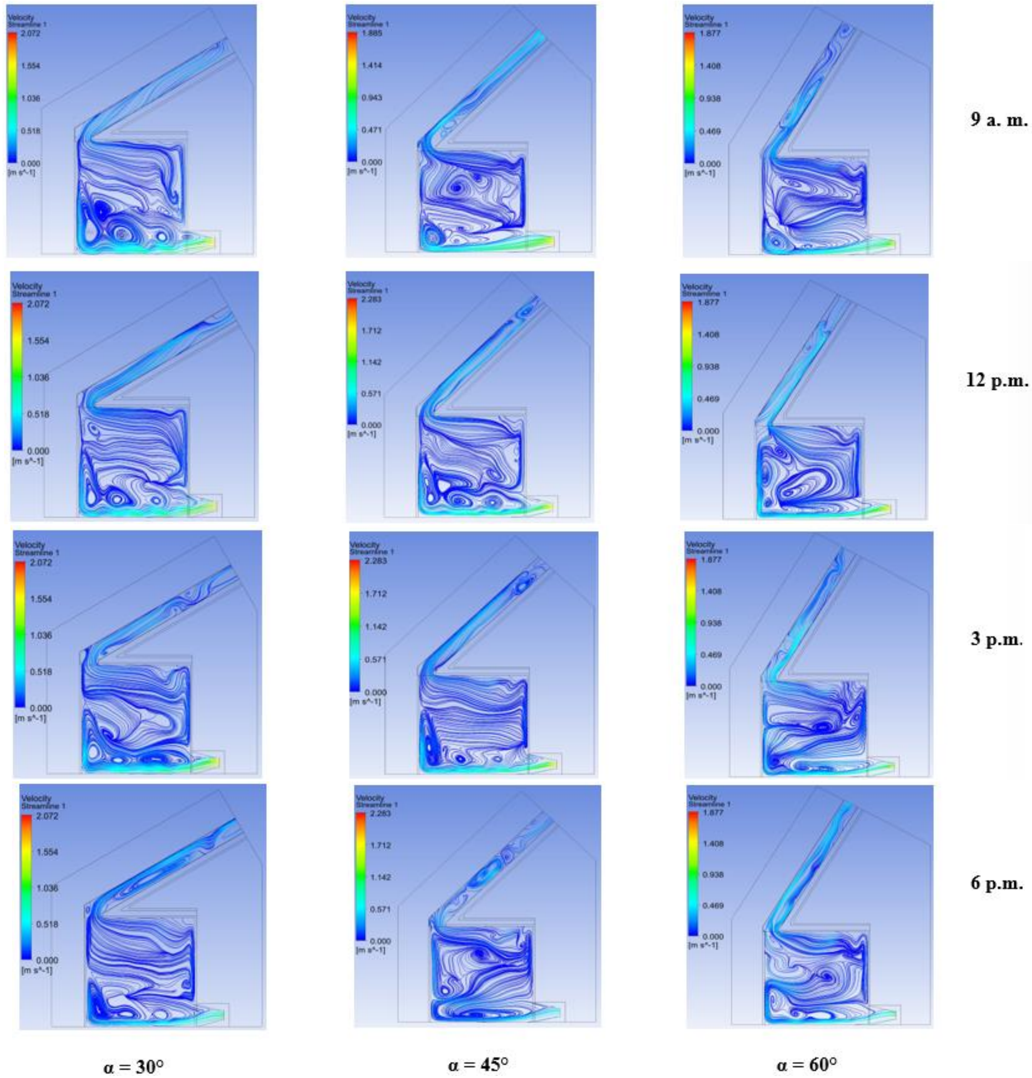

FIGURE 8. Contours illustrate the streamlines for the room and solar chimney at gab = 15 cm, different tilt angle of solar collector and with different time

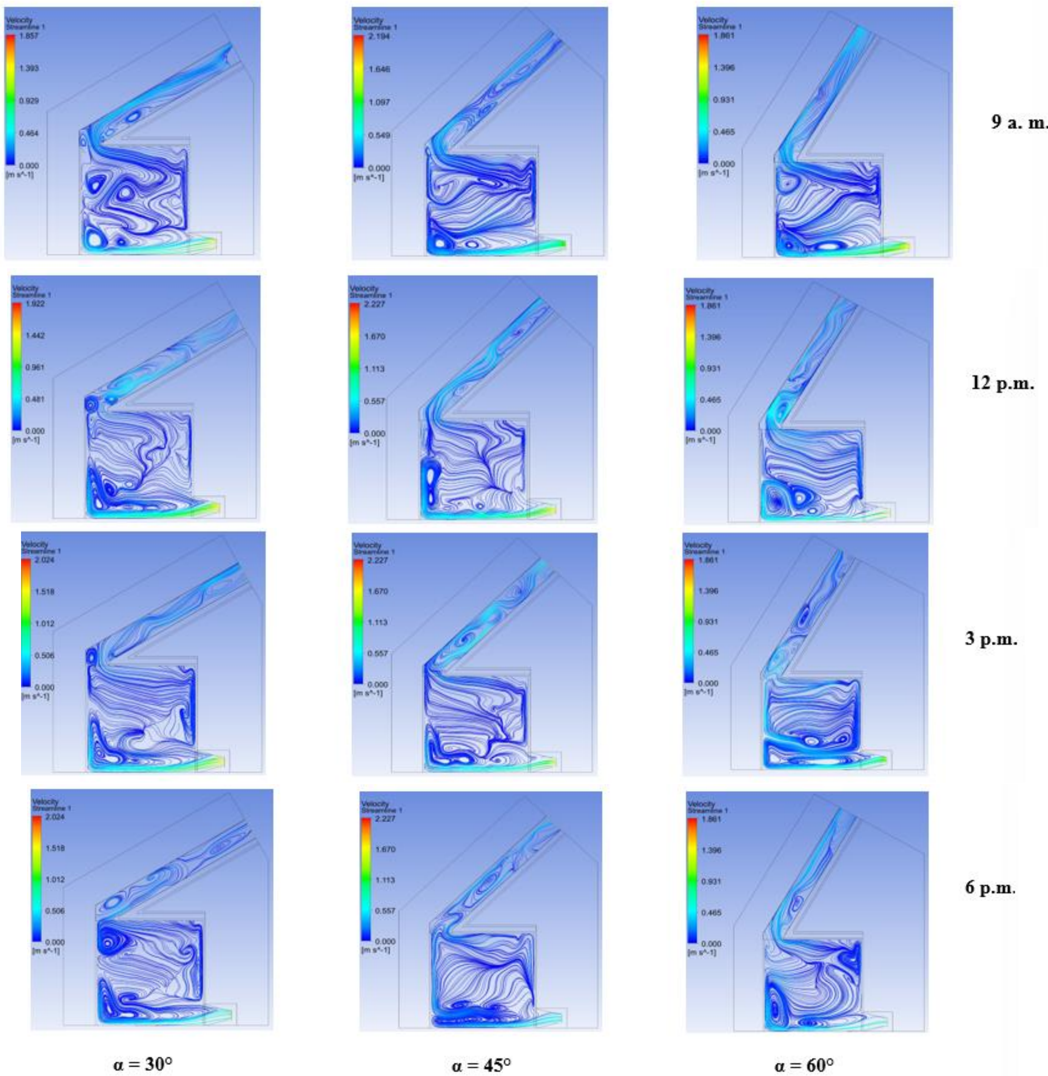

FIGURE 9. Contours illustrate the streamlines for the room and solar chimney at gab = 20 cm, different tilt angle of solar collector and with different time

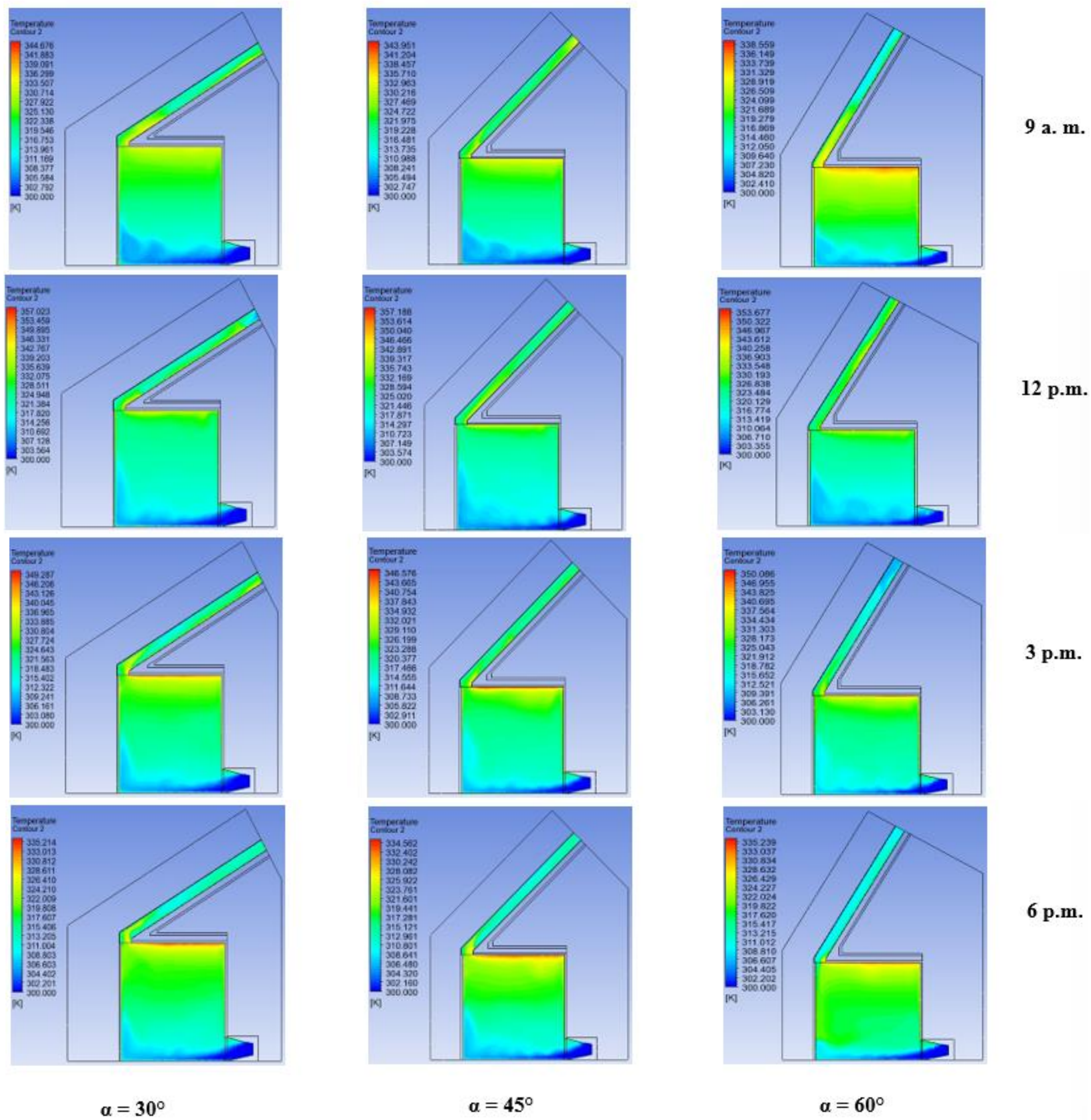

FIGURE 10. Contours illustrate the temperature for the room and solar chimney at gab = 10 cm, different tilt angle of solar collector and with different time

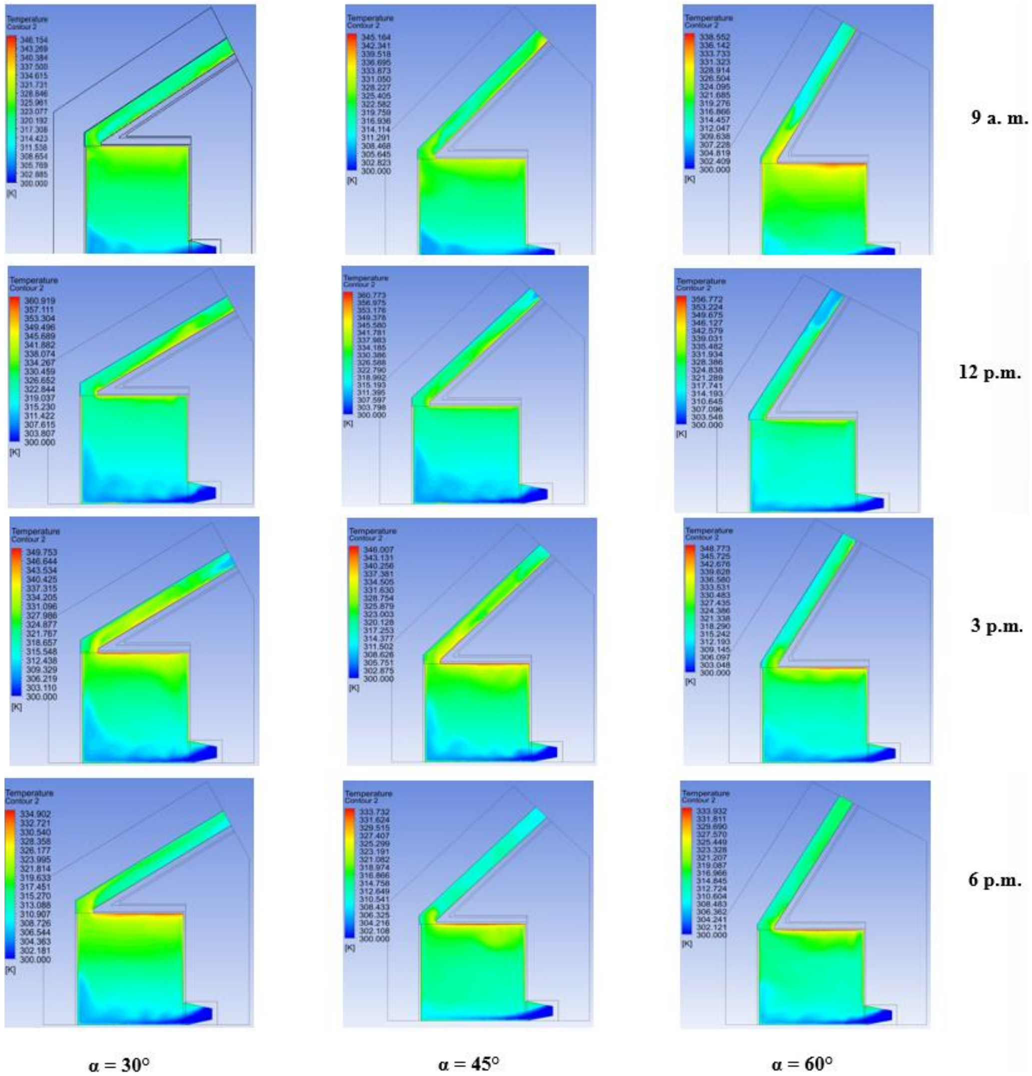

FIGURE 11. Contours illustrate the temperature for the room and solar chimney at gab = 15 cm, different tilt angle of solar collector and with different time

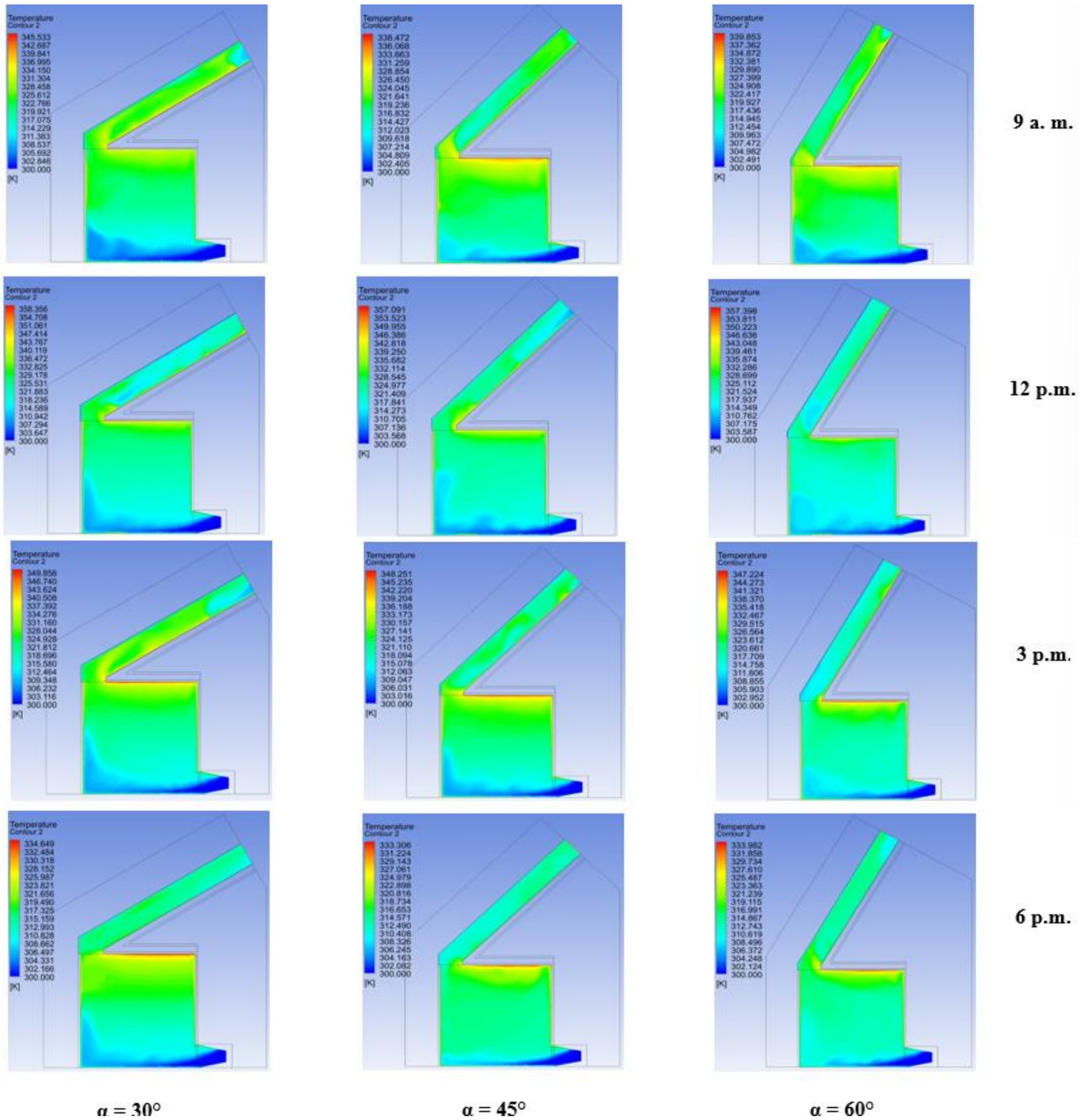

FIGURE 12. Contours illustrate the temperature for the room and solar chimney at gab = 20 cm, different tilt angle of solar collector and with different time

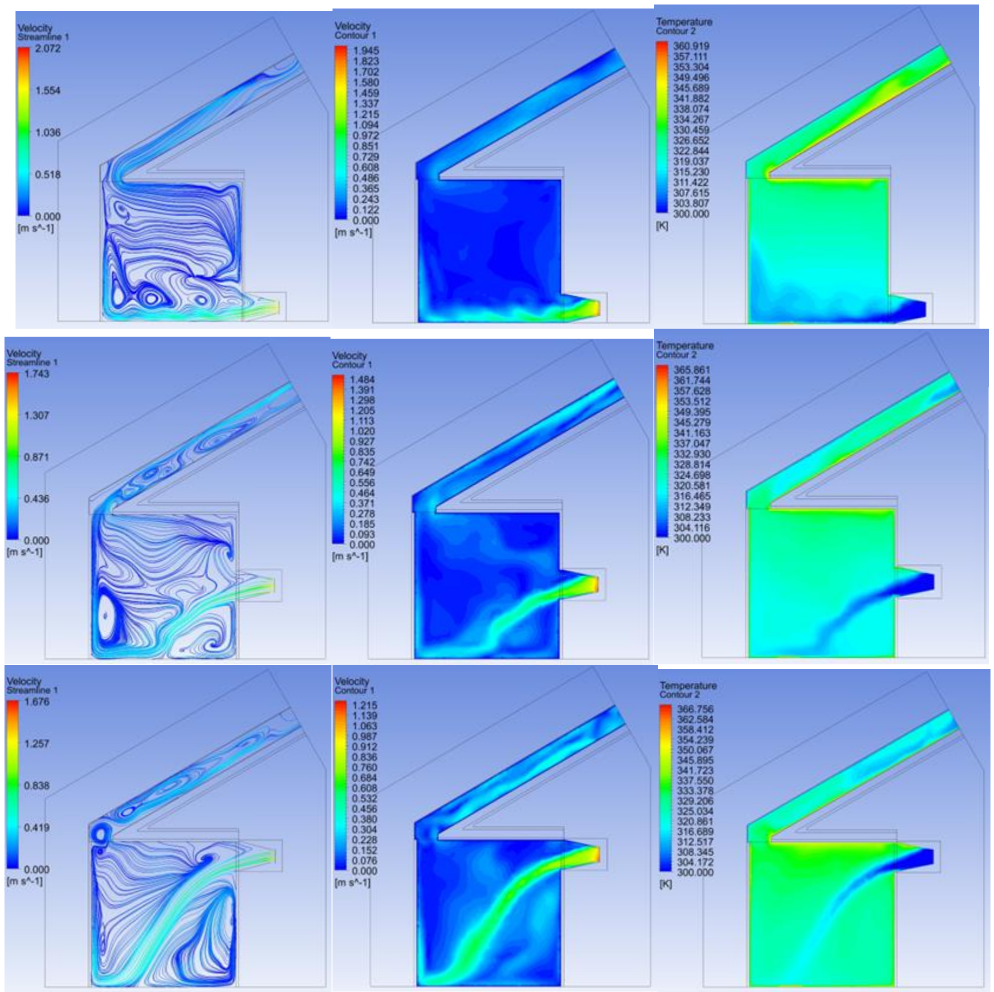

lower inlet

mid inlet

upper inlet

streamlines velocity temperature

FIGURE 13. Contours illustrate the effect of streamline velocity and temperature in the room and solar chimney for gab = 15 cm, α = 30° at 12 p.m

The temperature distribution for inlet solar chimney with time at different angles α = 30°, 45° and 60° and different gab 10 cm, 15 cm and 20 cm is shown in figure (14). Solar radiation penetrates the glass towards the heat-absorbing plate, heating the air, so it rushes out of the solar collector. The duration of heat exchange varies depending on the air gap and the angle of the solar collector, so there will be a temperature difference depending on the design. In (A) the minimum temperature inlet to solar collector at α = 30°, 9 a.m. (309.472 K) and the maximum temperature inlet at α = 45° at noon 12 p.m. (322.357 K), due to the varying air velocity owing to the different angle. The lowest inlet temperature at 45°, 6 p.m. (310.9 K), and the maximum inlet temperature to the solar collector is observed at angle 30° at 12 p.m. (319.569 K) as shown in (B), this change is due to the increase in the air gap. In (C) the minimum inlet temperature at 45°, 6 p.m. (311.246 K) and the maximum inlet temperature at 30°, 12 p.m. (316.929 K), then it decreasing until it reaches (311.805 K) at 6 p.m. For all shapes, the entry temperature decreases after 12 p.m. due to the decrease of solar radiation. From the previous figures, A, B and C, we notice that the highest inlet temperature is at angle 45° with air gap is 10 cm.

The plot of outlet temperature of solar chimney with time at different angles α = 30°, 45° and 60° and different gab 10 cm, 15 cm and 20 cm is shown in figure (15). Figure (15) – A and B shows the maximum outlet temperature of solar chimney at hours after noon, and for α = 30° this may be returned to increase the solar heat gain at this time. The angle 60° gives minimum outlet temperature of solar chimney, therefore, it can be selected the angle 30° to give maximum ventilation. Also, the gab 20 cm, α = 30° in (C) gives maximum temperature (more than 328 K).

The average velocity for outlet solar chimney with time at different angles α = 30°, 45° and 60° and different gab 10 cm, 15 cm and 20 cm is shown in figure (16). It can be notice from this figure A, B and C that the highest velocity rate of the solar chimney is at angle 60° (more than 0.4 m/s), and the lowest velocity rate at angle 30° (less than 0.2 m/s). This is due to the increased air gab; therefore, it causes a rise in temperature of mass flow rate at angle 30°.

Figure (17) shows the variation of solar radiation with time for three inclined angles (α = 30°, 45° and 60°) at gab 15 cm. The figure indicates the angle 30° and 45° gives maximum solar radiation (640 W/m^2) at the time of noon 12 p.m., for α = 30° and at afternoon 2 p.m., while the angle α = 60° gives low solar radiation.

The temperature distribution for inlet solar chimney with time at α = 30° and gab = 15 cm for different inlet location (lower, mid and upper) is shown in figure (18). It can be notes from the figure that the higher temperature distribution rate is when the inlet opening location is at the lower, and the lower temperature distribution rate is when the inlet opening location is at the upper due to decrease the ventilation (mass flow rates of air). Therefore, we choose the location of the lower inlet opening because it has the best ventilation rate.

The temperature distribution for outlet solar chimney with time at α = 30° and gab = 15 cm for different inlet location (lower, mid and upper) is shown in figure (19). It can be seen that the upper inlet location gives higher temperature distribution rate due to decrease the ventilation (mass flow rates of air), and when inlet opening located at lower gives the lower temperature distribution rate. Therefore, we choose the location of the lower inlet opening because it has the best ventilation rate.

The variation of average velocity for outlet solar chimney with time at α = 30° and gab = 15 cm for different inlet location (lower, mid and upper) is shown in figure (20). It can be seen from this figure that the higher average velocity is when the inlet opening location is at the lower, and the lower average velocity is when the inlet opening location is at the upper due to decrease the ventilation (mass flow rates of air). Therefore, we choose the location of the lower inlet opening because it has the best ventilation rate.

The effect of inclined angle (α = 30°, 45°, and 60°) on the ACH with time at gab = 10 cm as shown in figure (21). The ACH is started at approximate at time 8 a.m. and increase with time to become maximum at the time 11 a.m. due to rise the temperature of solar chimney that produce from increasing the solar radiation. Also, the figure shows that the angle 45° gives higher ACH.

The variation of inclined angle (α = 30°, 45°, and 60°) on the ACH with time at gab = 15 cm as revealed in figure (22). It can be seen from the figure that at angle 45°, the ACH reaches a maximum value of 54.0275 W/m^2 at 12 p.m., but at angle 30° the amount of air is greater during the day, at angle 60° the amount of ACH is the least possible at this air gap.

The effect of inclined angle (α = 30°, 45°, and 60°) on the ACH with time at gab = 20 cm as exposed in figure (23). The ACH is started at approximate at time 8 a.m. and increase with time to become maximum at the time 10 a.m. due to rise the temperature of solar chimney that produce from increasing the solar radiation. Also, the figure shows that the angle 45° gives higher ACH. And at α = 60°, gives the minimum of the ACH.

Figure (24) shows the effect of ACH with time at tilt angle α = 30° and for different gab of air for solar collector (gab = 10 cm, 15 cm, and 20 cm). It can be seen from this figure that the higher ACH is when the gab = 15 cm due to rise the temperature of solar chimney that produce from increasing the solar radiation. Also notice from the figure that the lowest amount of ACH is when the air gap of the solar chimney is 10 cm.

Figure (25) shows the effect of ACH with time at tilt angle α = 30° and gab = 15 cm for different inlet location (lower, mid, and upper). It can be seen that the upper inlet location gives higher ACH due to increase the solar radiation, and when inlet opening located at lower gives the lower ACH. Therefore, we choose the location of the lower inlet opening because it has the best ACH.

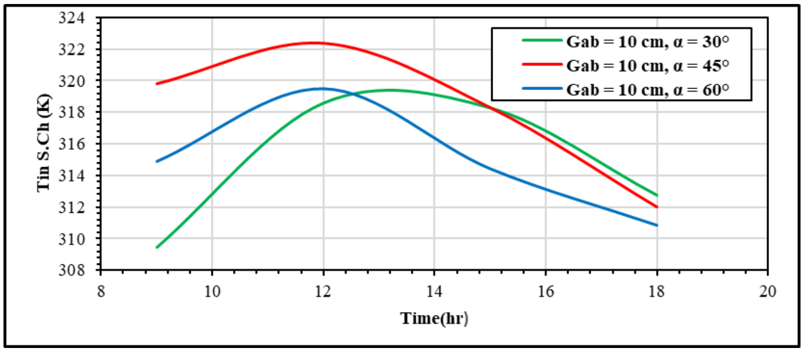

A.

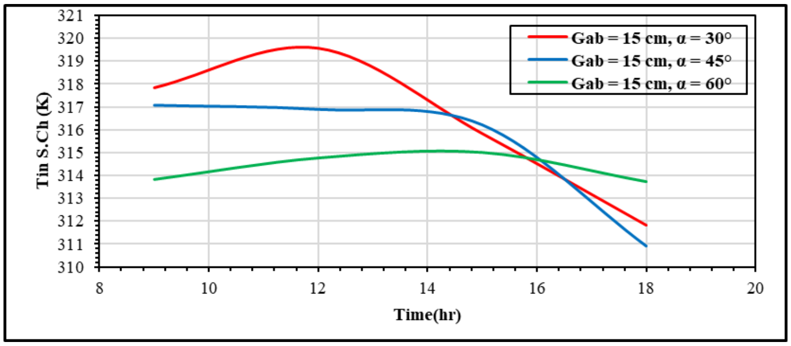

B.

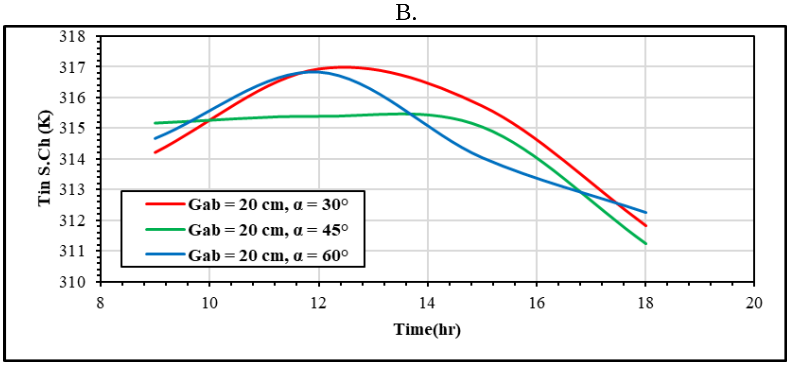

C.

FIGURE 14. Temperature distribution for inlet solar chimney with time: A. gab = 10 cm, B. gab = 15 cm, and C. gab = 20 cm with different tilt angle for solar chimney (α = 30°, 45°, 60°)

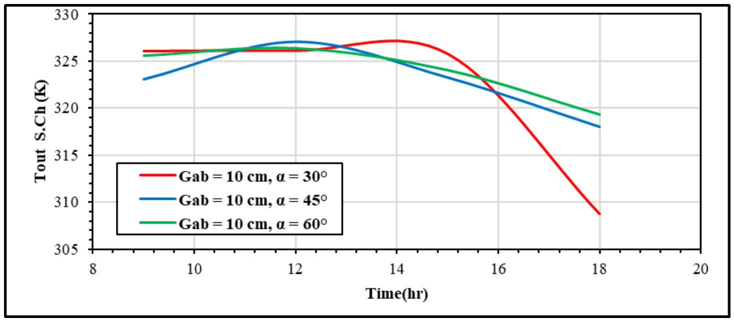

A.

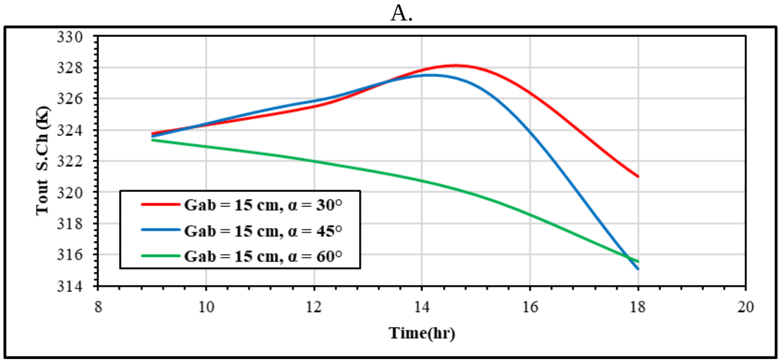

B.

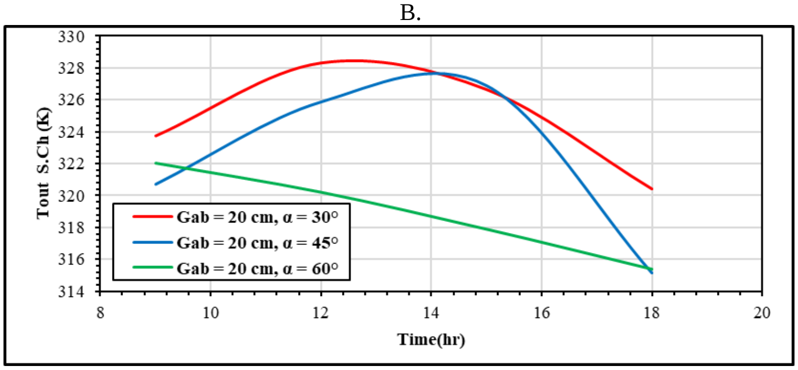

C.

FIGURE 15. Temperature distribution for outlet solar chimney with time: A. gab = 10 cm, B. gab = 15 cm, and C. gab = 20 cm with different angle for solar chimney (α = 30°, 45°, 60°)

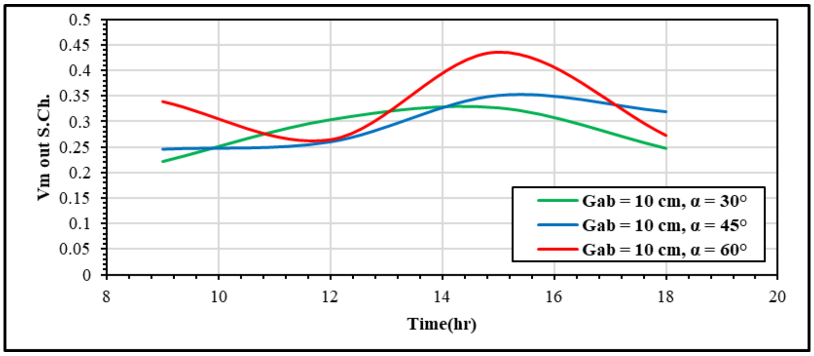

A.

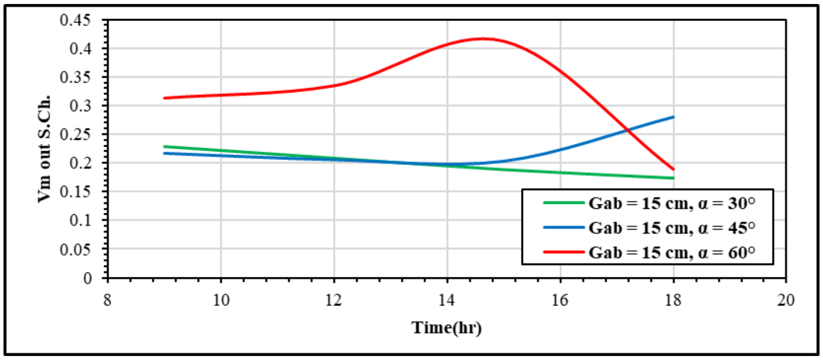

B.

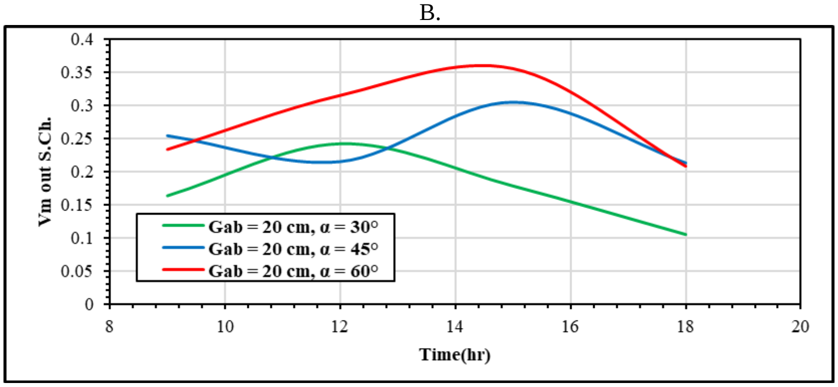

C.

FIGURE 16. Average velocity for outlet S.Ch. with time: A. gab = 10 cm, B. gab = 15 cm, and C. gab = 20 cm with different angle (α = 30°, 45°, 60°)

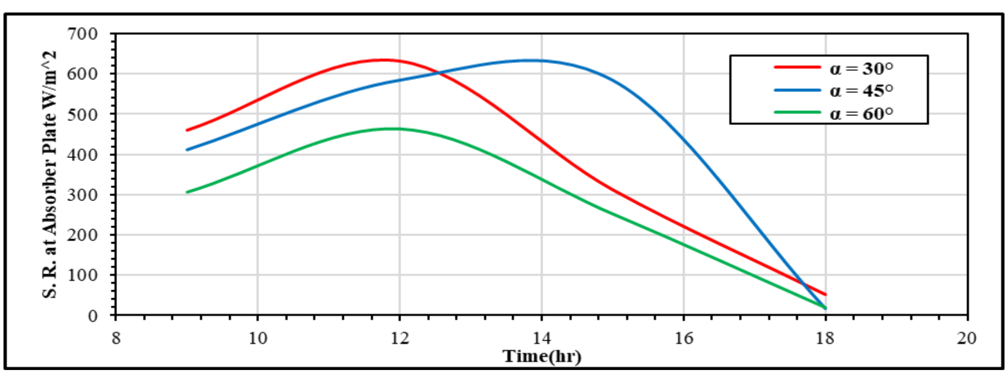

FIGURE 17. Solar radiation at absorber plate with time at gab = 15 cm and different angle for absorber plate α = 30°, 45°, 60°

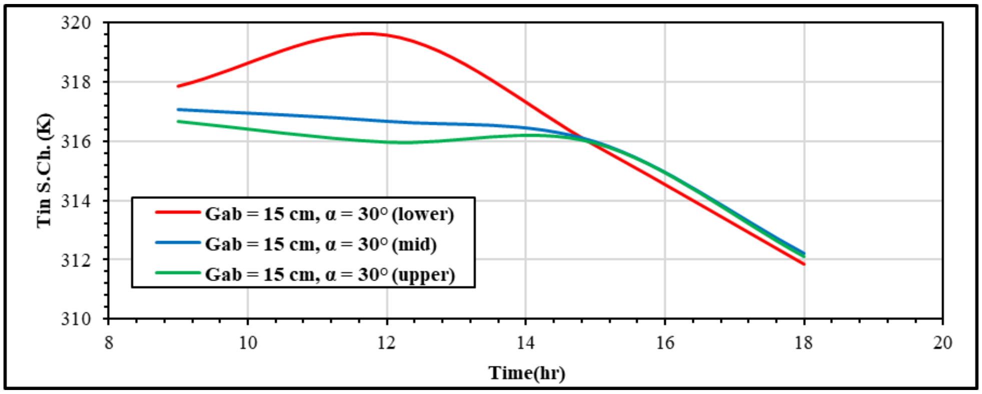

FIGURE 18. Temperature distribution for inlet solar chimney with time at: gab = 15 cm, and different inlet location: lower, mid, and upper

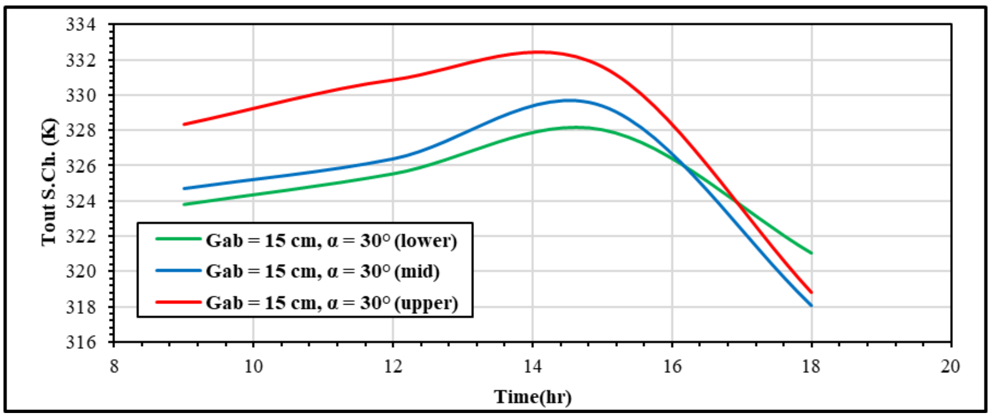

FIGURE 19. Temperature distribution for outlet solar chimney with time at: gab = 15 cm, and different inlet location: lower, mid, and upper

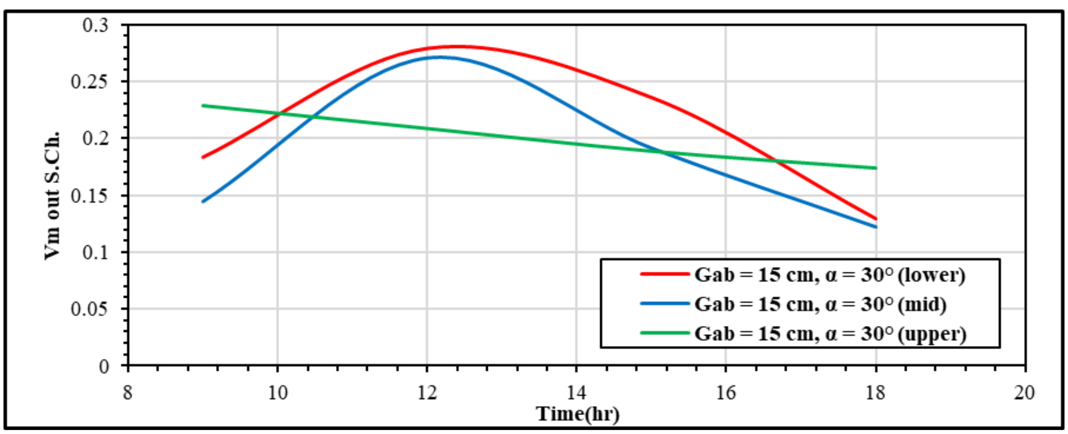

FIGURE 20. Average velocity for outlet solar chimney with time at gab = 15 cm and different inlet location: lower, mid, and upper

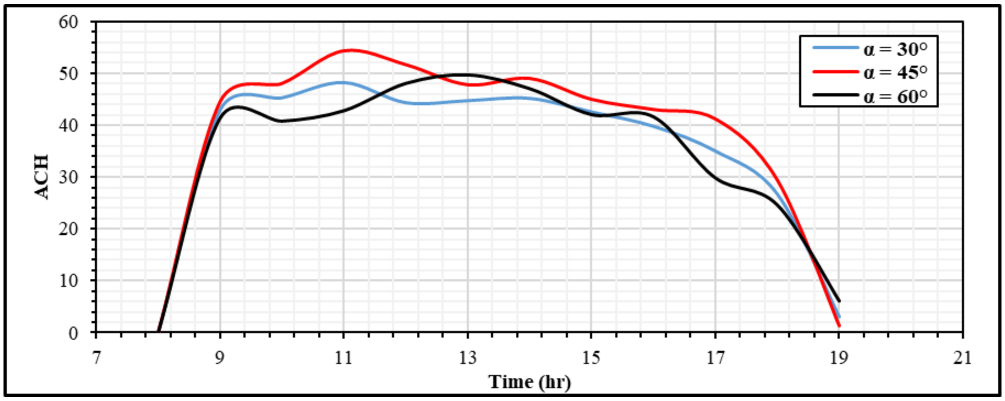

FIGURE 21. Air change per hour (ACH) with time at gab = 10 cm and different tilt angle of the solar chimney (α = 30°, 45°, 60°)

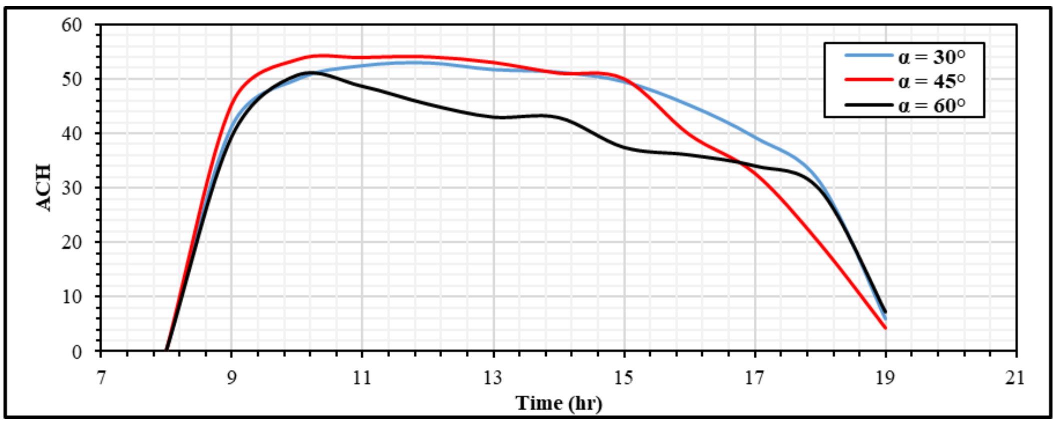

FIGURE 22. Air change per hour (ACH) with time at gab = 15 cm and different tilt angle of the solar chimney (α = 30°, 45°, 60°)

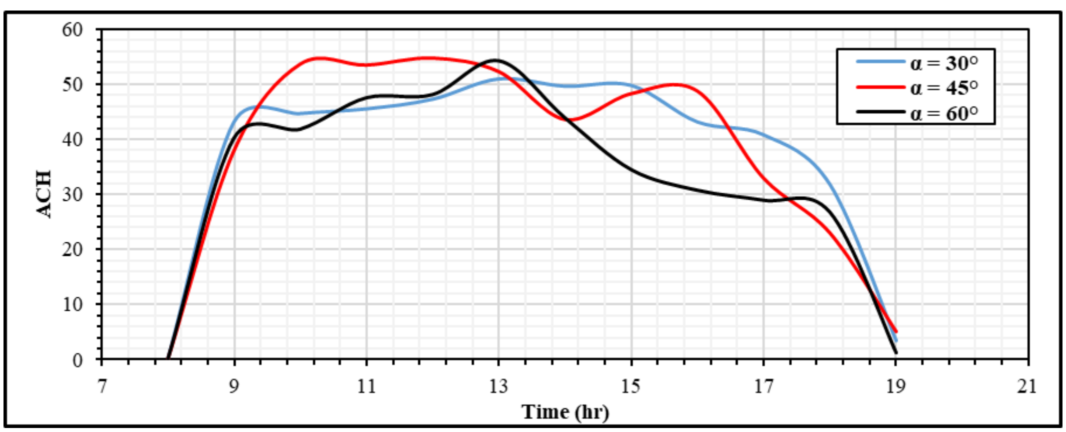

FIGURE 23. Air change per hour (ACH) with time at gab = 20 cm and different tilt angle of the solar chimney (α = 30°, 45°, 60°)

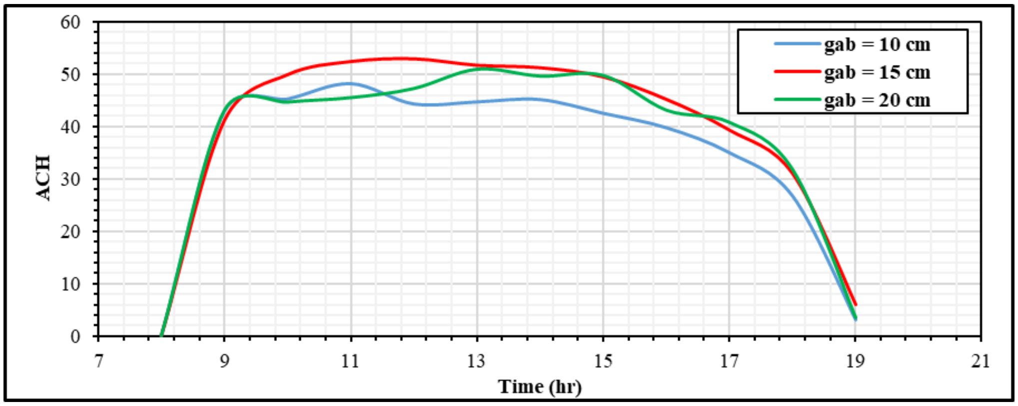

FIGURE 24. Air change per hour (ACH) with time at tilt angle of the solar collector α = 30° and different gab = 10 cm, 15 cm and 20 cm

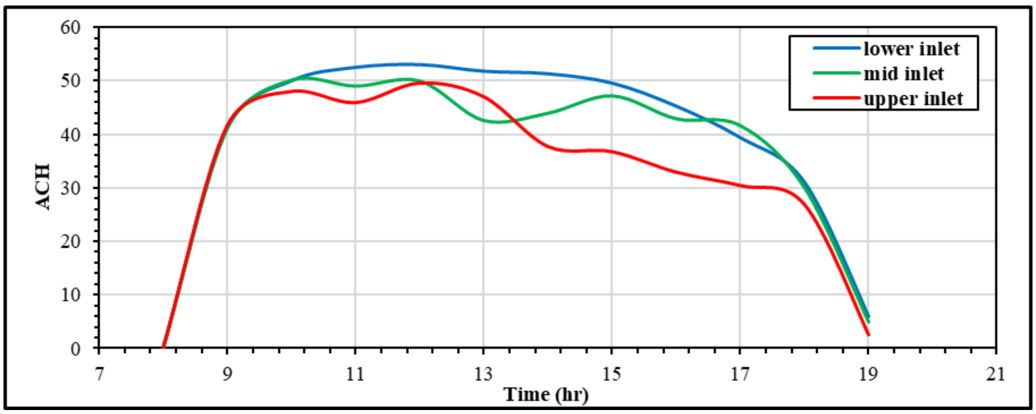

FIGURE 25. Air change per hour (ACH) with time at: tilt angle of the solar chimney α = 30°, gab = 15 cm, and different inlet location

CONCLUSION

In the present study, aimed at investigating the effect of solar chimney with the room is investigated in Basrah city, Iraq based on numerical and theoretical analysis. The numerical simulations were performed by using ANSYS – Fluent 2021/ R2. The effect of air gab for solar collector, the tilt angle of solar chimney, location of inlet opining, temperature and velocity for the solar chimney with room and air change per hour ACH was studied. The following conclusions were extracted:

- The optimum ratio of air gap width for solar chimney is 15 cm and tilt angle of solar chimney α = 30° to obtain the maximum ventilation rate and ACH.
- The solar radiation intensity had a very significant effect on flow rate and ACH.
- Basrah city annually records the highest amount of solar radiation during the months of June and July.
- The location of the air inlet opining at the lower floor for the room gives the best ventilation rate than the other inlet opening locations (mid and upper).
- The highest average temperature inlet to the solar collector is 322.357 K when the air gap is 10 = cm and the angle is 45°, and the lowest average temperature inlet the solar collector is found 309.472 K when the air gap is 10 = cm and the angle is 30°.
- The highest average temperature outlet for the solar collector is 328.326 K when the air gap is 20 = cm and the angle is 60° at 12 p.m., and the lowest average temperature outlet for the solar collector is found 315.115 K when the air gap is 15 = cm and the angle is 45°.

REFERENCES

1. I. Mehani and N. Settou, Passive Cooling of Building by using Solar Chimney (International Journal of Architectural and Environmental Engineering 6(9) 2012), pp.735-739.
2. R. M. Hannun, S. E. Najim and M. H. Khalaf, The Parameters Change with Different Operation Conditions of Solar Chimney Power Plant Model (Basrah Journal for Engineering Sciences 14(2) 2014), pp.189-199.
3. L. Shi, Theoretical models for wall solar chimney under cooling and heating modes considering room configuration, Energy 165, 925-938 (2018).
4. S. B. Abraham and T. Z. Ming, "Building's solar chimney: The performance of width and inlet to in tropical country," in International Conference on New Energy and Future Energy System-2019, IOP Conf. Series: Earth and Environmental Science 354, (IOP Publishing, Macau, China 2019), pp.012046.
5. A. Q. Mohamed, A. K. Alshara and H. M. Mitlaik, "Numerical study for the ventilation with solar chimney under effect of different location and the shape of the section opening window," in 3rd International Conference on Sustainable Engineering Techniques – 2020, IOP Conf. Series: Materials Science and Engineering 881 (IOP Publishing, Baghdad, Iraq, 2020), pp.012164.
6. H. J. Mohammed, A. J. Jubear and H. Obaid, Natural Ventilation in Passive System of Vertical Two-Stores Solar Chimney (Journal of Advanced Research in Fluid Mechanics and Thermal Sciences 69(2) 2020), pp.130-146.
7. H. Liu, P. Li, B. Yu, M. Zhang, Q. Tan, Y. Wang and Y. Zhang, Contrastive Analysis on the Ventilation Performance of a Combined Solar Chimney (Appl. Sci. 12(1) 2022), pp.156.
8. E. H. I. Cisse, B. A. Ndiogou1, S. Tigampo, A. Thiam and D. Azilinon, Optimization of a Solar Chimney with a Horizontal Absorber for Building Ventilation: A Case Study (FDMP 19(4) 2023), pp.901-910.
9. S. Yue, Z. Ge, J. Xu, J. Xie, Z. Xie, S. Zhang, and J. Li, Analysis of the Ventilation Performance of a Solar Chimney Coupled to an Outdoor Wind and Indoor Heat Source (Appl. Sci. 13 ,2023), pp.2585.
10. R. Bassiouny, N. S.A. Koura, An analytical and numerical study of solar chimney use for room natural ventilation (Energy and Buildings 40 ,2008), pp.865–873.
11. H. Li, Y. Yu, F. Niu, M. Shafik, and B. Chen, Performance of a coupled cooling system with earth-to-air heat exchanger and solar chimney (Renewable Energy 62 ,2014), pp. 468-477.
12. A. H. Poshtiri1, N. Gilani, and F. zamiri, "Feasibility study on using solar chimney and earth-to-air heat exchanger for natural heating of buildings," in World Renewable Energy Congress-2011, Low Energy Architecture (LEA), (Linkoping, Sweden, 2011), pp.1773-1780.
13. F. M. Abed, M. H. Zaidan, Y. H. Hussein and A. K. Jassim, "Passive air-conditioning of domestic using a hybrid system of solar updraft tower and a geothermal in Tikrit city-Iraq," in STEPS-2020, IOP Conf. Series: Materials Science and Engineering 1058 (IOP Publishing, Erbil, Iraq, 2021), pp.012057.
14. M. Nakielska and K. Pawłowski, "Increasing natural ventilation using solar chimney," in E3S Web of Conferences-2017, Energy and Fuels 14 (EDP Sciences, 2017), pp. 01051.
15. A. A. Serageldina,b , A. K. Abdelrahmanb and S. Ookawarac, Parametric study and optimization of a solar chimney passive ventilation system coupled with an earth-to-air heat exchanger (Sustainable Energy Technologies and Assessments 30 ,2018), pp. 263–278
16. M. A. Abdel-Baky, E. I. Eaid, I. A. El-Khaldy and A. F. Tawfic, Investigation of natural ventilation using a solar chimney in various solar cases (International Journal of Innovative Research and Scientific Studies 7(2), 2024), pp. 587-606.
17. X. Jianliu and L. Weihua, Study on solar chimney used for room natural ventilation in Nanjing (Energy and Buildings 66, 2013), pp. 467–469.
18. R. Bassiouny and N. S.A. Korah, Effect of solar chimney inclination angle on space flow pattern and ventilation rate (Energy and Buildings 41 ,2009), pp. 190–196.
19. B. Buonomo, L. Capasso, A. Diana, O. Manca and S. Nardini, "A numerical analysis on a solar chimney with an integrated latent heat thermal energy storage," in 74th ATI National Congress-2019, AIP Conference Proceedings 2191, (AIP Publishing, Modena, Italy, 2019), pp.020029.
20. H. K. Versteeg and W. Malalasekera, An Introduction to Computational Fluid Dynamics (Pearson Education Limited, England, 1988).
21. A. Pasupathy, L. Athanasius, R. Velraj and R.V. Seeniraj, Experimental investigation and numerical simulation analysis on the thermal performance of a building roof incorporating phase change material (PCM) for thermal management (Applied Thermal Engineering 28, 2008), pp.556–565.

22. B. E. Launder and D. B. Spalding, The Numerical Computation of Turbulent (Computer Methods in Applied Mechanics and Engineering 3,1974), pp. 269-289.
23. Y. H. Qian and S. A. Orszag, Lattice BGK Models for the Navier-Stokes Equation: Nonlinear Deviation in Compressible Regimes (Europhysics Letters 21(3), 1993), pp. 255-259.
24. Ansys, C. F. X. "Release 11.0." ANSYS CFX-solver theory guide, ANSYS (2006).
25. A. M. Salman, A. A. Monem and E. A. Khazal, Indoor Air Quality in a Cardiac Care Unit (CCU) under Different Ventilations (Basrah Journal for Engineering Sciences 21(1), 2021), pp.1-7.
26. Z. Shia, J. Chena and Q. Chen, On the turbulence models and turbulent Schmidt number in simulating stratified flows (Journal of Building Performance Simulation 9(2), 2016), pp.134-148.
27. H. Awbi, Ventilation of Buildings (Taylor & Francis, New York, 2003).
28. B. K. Soni, J. F. Thompson and N. P. Weatherill, Handbook of Grid Generation (CRC Press LLC, USA,1999).
29. J. Mathur, N.K. Bansal, S. Mathur, M. Jain and Anupma, Experimental investigations on solar chimney for room ventilation (Solar Energy 80, 2006), pp. 927–935.
30. D. Park, “The Application of the Solar Chimney for Ventilating Buildings,” Ph.D. thesis, the faculty of the Virginia Polytechnic Institute and State University, 2016.